Vol. 04 No. 01 2026

RiESTech

JOURNAL RECENT IN ENGINEERING SCIENCE AND TECHNOLOGY

MBI

E- ISSN : 2985-8321
P -ISSN : 2985-704X

Recent in Engineering Science and Technology (RiESTech)
PT MENCERDASKAN BANGSA INDONESIA (MBI)
Available online at: http://www.mbi-journals.com/index.php/riestech

E- ISSN : 2985-8321
P -ISSN : 2985-704X

Recent in Engineering Science and Technology (RiESTech)

Volume 4 No 1 January 2026

FOCUS AND SCOPE

RIESTECH

Recent in Engineering Science and Technology **(RiESTech):** I*SSN: 2985-704X (print), ISSN: 2985-8321 (online)* a peer-reviewed quarterly engineering journal, publishes theoretical and experimental high-quality papers to promote engineering and technology's theory and practice. In addition to peer-reviewed original research papers, the Editorial Board welcomes original research reports, state-of-the-art reviews, and communications in the broadly defined field of recent engineering science and technology. **RiESTech** covers topics contributing to a better understanding of engineering, material science, computer science, environmental science, and their applications. **RiESTech** is concerned with scientific research on mechanical and civil engineering, Electrical/Electronics and Computer Engineering, and Metallurgical and Materials Engineering with specific analytical techniques and/or computational methods.

The frequency of RiESTech publications is four times a year namely in January, April, July, and October. The scope of RiESTech includes a wide spectrum of subjects namely:

Mechanical and Civil Engineering (Automotive Technologies; Construction Materials; Design and Manufacturing; Dynamics and Control; Energy Generation, Utilization, Conversion, and Storage; Fluid Mechanics and Hydraulics; Heat and Mass Transfer; Micro-Nano Sciences; Renewable and Sustainable Energy Technologies; Robotics and Mechatronics; Solid Mechanics and Structure; Thermal Sciences)

Electrical/Electronics and Computer Engineering (Instrumentation; Coding, Cryptography, and Information Protection; Communications, Networks, Mobile Computing, and Distributed Systems; Compilers and Operating Systems; Parallel Processing, and Dependability; Computer Vision and Robotics; Control Theory; Electromagnetic Waves, Microwave Techniques and Antennas; Embedded Systems; Integrated Circuits, VLSI Design, Testing, and CAD; Microelectromechanical Systems; Microelectronics, and Electronic Devices and Circuits; Power, Energy and Energy Conversion Systems; Signal, Image, and Speech Processing; Machine Learning and Data Science)

E- ISSN : 2985-8321
P -ISSN : 2985-704X

Metallurgical and Materials Engineering (Advanced Materials Science; Ceramic and Inorganic Materials; Electronic-Magnetic Materials; Energy and Environment; Materials Characterization; Metallurgy Extractive; Polymers and Nanocomposites)

Environmental Science and Engineering (Waste Management, Climate Change, Zero Waste, Environmental Disaster Management, Circular Economy, Sustainable Development, Environmental Security, Environmental Management, Environmental Ecology, Conservation of Natural Resources And Environment, Environmental Impact Analysis, Planning and Environmental Administration, Environmental Health, Environmental Pollution, Environmental Accounting, and Environmental Information Systems)

Recent in Engineering Science and Technology (RiESTech)
PT MENCERDASKAN BANGSA INDONESIA (MBI)
Available online at: http://www.mbi-journals.com/index.php/riestech

E- ISSN : 2985-8321
P -ISSN : 2985-704X

Recent in Engineering Science and Technology

(RiESTech)

Volume 4 No 1 January 2026

E- ISSN : 2985-8321
P -ISSN : 2985-704X

Layout and Typesetting:

Imam Sapto Nugroho, Universitas Indonesia (Alumni), Indonesia
Kamil Raihan Permana, Universitas Indonesia, Indonesia
Raihan Trinanda Agsya, Politeknik Negeri Jakarta, Indonesia

PUBLISHER
PT MENCERDASKAN BANGSA INDONESIA (MBI)
Address : 4th Floor Gedung STC Senayan Room 31-34, Jl. Asia Afrika Pintu IX, Jakarta 10270, Indonesia.

Recent in Engineering Science and Technology (RiESTech)
PT MENCERDASKAN BANGSA INDONESIA (MBI)
Available online at: http://www.mbi-journals.com/index.php/riestech

E- ISSN : 2985-8321
P -ISSN : 2985-704X

Recent in Engineering Science and Technology (RiESTech)

Volume 4 No 1 January 2026

PREFACE

Journal RiESTech (p-ISSN: 2985-704X (print), e-ISSN: 2985-8321 (online); is a peer review journal published by PT Mencerdaskan Bangsa Indonesia. The RiESTech journal is published four times a year in January, April, July, and October. This journal provides direct open access to its content on the principle that making research freely available to the public supports a greater global exchange of knowledge within the engineering field. This journal aims to provide a place for academics, researchers, and practitioners to publish original research articles or review articles. The scope of articles published in this journal relates to various topics in the field of outcomes of research activities.

The RiESTech journal publishes papers strictly following the RiESTech guidelines and templates for manuscript preparation. All submitted manuscripts will go through a double-blind peer review process. The paper is read by members of the editor (according to the area of specialization) and will be screened by the Managing Editor to meet the criteria required for RiESTech publication. Manuscripts will be sent to two reviewers based on their historical experience in reviewing manuscripts or based on their areas of specialization. RiESTech has review forms to keep the same item reviewed by two reviewers. Then the editorial board makes a decision on the comments or suggestions of the reviewers.

Reviewers provide an assessment of originality, clarity of presentation, contribution to the field/science. This journal publishes research articles, review articles/literature reviews, case reports and concept/policy articles, in all fields of Computer Science, Informatics Engineering, Multimedia, Arts. The article to be published is an original work and has never been published. Incoming articles will be reviewed by the reviewer team.

The Editorial Board will try to continue to improve the quality of the journal so that it can become an important reference in the development of engineering sciences. The greatest appreciation and gratitude to Mitra Bestari along with members of the Editorial Board and all parties involved in the publication of this journal. Complete writing instructions are displayed on the portal of this journal.

Regards,

Chief Editor

Recent in Engineering Science and Technology (RiESTech)
PT MENCERDASKAN BANGSA INDONESIA (MBI)
Available online at: http://www.mbi-journals.com/index.php/riestech

E- ISSN : 2985-8321
P -ISSN : 2985-704X

Recent in Engineering Science and Technology (RiESTech)

Volume 4 No 1 January 2026

Contents

Articles

RiESTech
Recent in Engineering Science and Technology

MBI

Article

CLIMATE CHANGE – GREEN BLAST FURNACES

Nicholas Standish [1*]

[1] Emeritus Professor University of Wollongong, Northfields Ave Wollongong, NSW 2522, Australia
* Correspondence: mst97899@gmail.com

Abstract: Recent paper on Climate Change in this journal considered Green Steel and argued for a DRI-EAF route using charcoal from tree branches in forest plantations that are maintained by workers using hand tools. And this will continue even more in proposing charcoal's major use in blast furnaces. There are many operating iron blast furnaces in Indonesia and worldwide using coke and as the process is capital intensive they must be operated for a long time. This means that most blast furnaces with their coke ovens will continue producing iron and large amounts of CO_2 for many years yet, making zero carbon unattainable. An obvious question is: Can coke in the iron blast furnace be substituted by the more climate friendly charcoal? And if yes, will it be economic and will the blast furnace be as productive as now? Following an exhaustive literature study this paper answers the question positively. It is demonstrated that there are two fundamentally different requirements of carbon in blast furnaces that people have not appreciated and instead followed a hundred year tradition in treating them as one. This paper exposes them as two different carbons, namely: the cohesive zone carbon and the shaft zone carbon. This is perhaps the first time that this has been done, as so far these two quite different evidence-based theory requirements of a blast furnace carbon have been invariably introduced as a single carbon, namely: coke in coke BFs and charcoal in charcoal BFs. It is also demonstrated that large blast furnaces can operate with this dual carbon burden not too differently from a 100% coke or a 100% charcoal carbon burdens. It is also good economics as cheaper charcoal is substituted for expensive coke.

Keywords: Indonesia; Charcoal; GHG emission; Blast furnace; Cohesive zone

Citation: Standish, N. (2026). CLIMATE CHANGE – GREEN BLAST FURNACES. Recent in Engineering Science and Technology, 4(01), 1–21. Retrieved from https://www.mbi-journals.com/index.php/riestech/article/view/145

Academic Editor: Noor Hidayati

Received: 1 December 2025
Accepted: 15 January 2025
Published: 31 January 2026

Publisher's Note: MBI stays neutral with regard to jurisdictional claims in published maps and institutional affiliations.

1. Introduction

It is well documented that the amount of CO_2 generated since the start of industrial revolution has been rising. This rise was kept at bay by the two earth's natural sinks, namely land sink (forests and agriculture) and water sink (oceans and lakes). However, as forests were cut down for timber and to free land for houses and industry the land sink has been steadily decreasing and reducing its ability to absorb more and more of the CO_2 generated, so the CO_2 content in the atmosphere has been rising over time.

Many climate scientists believe that increased CO_2 will cause amplified global warming and more extreme weather events affecting human health. Be that as it may, but right now more CO_2 closer home is definitely a problem in accelerating materials' corrosion and causing "concrete cancer' – and with high humidities in Indonesia even more so!

The recently published paper titled Climate Change in Indonesia: Green Steel [1], strongly argued for a DRI-EAF route using charcoal from tree branches in forest plantations that are maintained by workers using hand tools and create millions of jobs throughout the country.

Using charcoal makes a lot of practical sense because this way we get double benefit – one: increasing CO_2 absorption by forests by not cutting trees down and two: decreasing

the overall CO_2 of the DRI process by regenerating the emitted CO_2 with charcoal and reusing the so-formed CO.

For Indonesia this has much higher benefit still because its AFOLU (Agriculture, Forestry and Other Land Use), at 53% emission [2] is just more than double that of the worldwide average of 24% [3].

Commenting on this, Zaki [3] also said "It is ironic that forests, which should serve as carbon sinks, have instead become major emission sources due to land burning, forest conversion, and peat degradation."

Over the years in Indonesia there have been many forest laws issued that should have stopped their degradation, but they were apparently not strong enough legally [4] so degradation continued. Hopefully the Presidential Regulation No. 5/2025 of 21 January 2025 on Forest Area Management, issued by President Prabowo and creating a new task force headed by the defense minister, the TNI commander and the attorney general will be effective. As expected this law has its critics cautioning that it militarizes environmental governance and risks repressing communities defending their land.

It should be pointed out that President Prabowo continues making efforts to see Indonesia reduce its GHG (Green House Gas) emission as quickly as possible; he even reduced the zero target year from its 2060 to 2050 at the G20 Summit 2024 in Brazil (to be reversed back again to 2060), and right now (October 2025) President Prabowo announced full support for Brazil's TFFF (Tropical Forest Forever Facility) by stating: "Brazil has established an investment fund that aims to conserve tropical forests. Brazil pioneered this movement, and we support it. We will commit whatever amount Brazil has invested there Indonesia will invest here." [Note: TFFF aims to set up a $125 billion global investment fund to provide tropical countries with permanent income in exchange for protecting their forests].

To sum up so far. AFOLU emissions released by lands and forests in Indonesia produce twice as much greenhouse gases than other emissions and reducing them via charcoal in making iron and steel gives twice the benefit. As was demonstrated in the recent paper [1], this can be done immediately for DRI production and assisted by hydrogen if it is economic.

However, there are many operating iron blast furnaces worldwide using coke - some are new and some are being relined right now at high cost. For example in Australia, Bluescope Steel has announced in October 2025 a reline of its Port Kembla No 6 BF at a cost of $1.15 billion.

The reason for this is that the BF process is capital intensive, and to be cost effective it must be operated for a long time or to use the ironmaking terminology, have a "long campaign". Modern BFs have campaign lives of 20 years, or more.

Economically this means that most blast furnaces with their coke ovens will continue producing iron and large amounts of GHG emissions, making zero carbon targets unattainable.

The question is: can coke in the iron blast furnace be substituted by charcoal? And if yes, will it be economic and will the BF be as productive as now? The answer is yes! It has been done in Brazil for decades in small size blast furnaces. For example, in 2020 – 31.42 million tonnes came from integrated mills using charcoal. [5]. One BF of 350 m^3 or cum, is producing 600 tpd of iron. By contrast, modern coke blast furnaces are 2,000 – 6,000 cum producing 5,000 – 15,000 tpd (tonnes per day) of iron.

Therefore, we need to establish if coke can technically be substituted by charcoal in existing blast furnaces, most of which are large, and whether it can be done by a full

substitution as in Brazil or not, and how effective and economic these substitutions are likely to be.

2. TECHNICAL BACKGROUND

To establish if coke can technically be substituted by charcoal, we start with first principles.

The basic principle, as pointed out in the previous paper [1], is that no matter how, or where you do it - to make iron from its ore, generally hematite, Fe_2O_3, you need to remove its oxygen, and for every one tonne of Fe made this requires theoretically 161 kg of carbon, or in actual practice to account for losses, inefficiencies, incomplete reactions, etc about double that. As quantities under ideal conditions may interfere with final conclusions – and are simple to calculate from standard chemical stoichiometry and thermodynamics, we will postpone quantities till later, and go directly to essential basics and industrial data to support answers to our question.

2.1 Blast Furnace

A Blast Furnace (BF) is a tall cylindrical furnace. Layers of small size iron ore (6-20mm) and large size coke (25-60mm) are charged at the top and move down counter to upcoming hot, reducing gases, generated in the bottom. Much of the carbon's chemical energy is not fully used in reduction and leaves the BF as CO. Ore particles in moving down, are reduced, then melted in the bottom and the molten iron collected in the hearth to be periodically tapped.

These materials form alternating layers in the furnace and are supported on a bed of incandescent coke below. Hot air at high pressure is blown into the lower part of the furnace. The coke combusts, producing heat and carbon monoxide (CO) gas which passes through the porous bed. The CO removes the oxygen from the iron ore forming CO_2 and the heat melts the charge, producing hot metal.

Hot metal is a solution of molten iron at approximately 1480 °C, which contains 4 percent carbon and some other elements like Si, Mn, Ti, etc. This hot metal flows to the bottom of the furnace, through the coke bed and is periodically "tapped" from the furnace into torpedo cars and transported to the BOF shop where it is refined into steel.

A traditional Blast Furnace Plant consists of five major parts 1 – The Blast Furnace itself, 2 – The Coke Ovens, 3 – The Stoves, heated by the BFG (Blast Furnace Gas) assisted by the richer COG (Coke Oven Gas) to increase the blast temperature to as high as 1300°C, 4 – The Slag Granulation and on-treatment sold as clinker for cement making, and 5 – The Stockhouse, to store, blend and send materials to the top BF charging gear, historically bells, but since 1975 BLT (Bell-Less Top). This, plus tuyere injection, high top pressure and its TRT (Top pressure Recovery Turbine), enhanced control architecture, etc, are designed to save the expensive coke of some $US500/tonne.

2.1.1. Subsidiary Notes

1) Blast furnaces are tall, about 50m all up. This why in all countries – except English! – it is called Hochoffen,고로, Alto Horno, Vysoka Peč, 高炉, Haut Fourneau, etc. 2) BFs are always tall – irrespective of production quantities, and the reason is what I call "cooking time", which means under the blast furnace conditions, starting with 'raw' particles (iron oxide) and finish with 'ripe' particles (iron metal) it takes the same time. Blast furnace production is then obtained by increasing the furnace cross-sectional area. 3) DRI reactors, e.g. Midrex, Hylsa, etc, are essentially blast furnace shafts, and are also tall for the same reason. 4) Ferrous burden (pellets, sinter or lump ore) size is small because its usual (economic) reducibility has always been the norm. It is true that reducibility of natural ores are fixed over a narrow band, but reducibility of sinter and pellets can be varied over a wide range. 5) BF coke size is large because its usual (traditional) physical properties have always been the norm. Coke is the only raw material

that descends into the lower part of the blast furnace (BF) in its original form; therefore, it is of utmost importance to improve the coke properties for its use in BF.

From all of the above information we can conclude that:

The BF is essentially a heat engine + chemical reactor — with useful output of gas energy. When talking of blast furnaces, I like to stress that to really understand it we must look at the blast furnace in a number of its roles. This is shown in a series of following figures.

2.2. Physical Blast Furnace

Figure 1 is what I call a physical BF. It shows: "Granular zone" also called "lumpy zone", cone-shaped "Cohesive zone" with its "coke slits' or 'coke windows', "Active coke zone" and "Stagnant coke zone", better known as 'deadman'. It is important to thank our Japanese colleagues who shared their findings of quenched operational blast furnaces – eight with water and one with nitrogen – starting with Higashida in 1968.

The finding of the greatest importance is that all furnaces showed that layers of ore and coke, set at the stockline on the top do not mix but remain as layers right to the bottom.

The second finding of great importance was that all furnaces, showed an existence of a cohesive zone of different shapes.

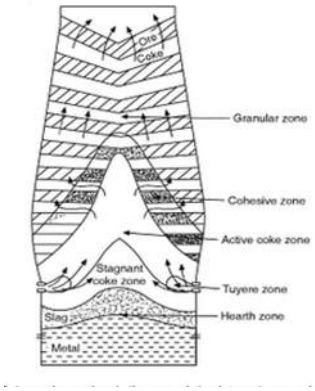

Figure 1. Physical BF

Subsequent quenched furnaces, including one of best productivity, showed that the best shape is an inverted V-shape, or cone. Incidentally, the best way to ensure a good conical shape is to get a central gas flow, which in practice means to charge large coke in the centre. It is also essential to ensure that an equal blast from each tuyere is maintained, otherwise the inverted cone becomes deformed in some way and furnace productivity suffers.

From the fundamentals of fluid flow that fluids always flow from high to low pressure, a horizontal jet of fluid, in our case gas from tuyeres, will always take a curved path to the lower pressure at the top AND from the basics of granular materials a horizontal jet of gas aimed at a granular mound is like hitting a semi-solid wall, so it gives in and goes up and at the next open 'window' does 'a dog leg' to flow to the top following a path of least resistance.

Figure 2. Cohesive zone. Chiba No 2

Figure 2 is a photo of an actual cohesive zone in an actual operating BF after water quenching and excavating the burden. In showing this photo, I need to thank the former Kawasaki Steel Company for allowing me to use it for educational purposes.

It shows the quenched Chiba No 2 after it was excavated and a slice of its stack cut off, and a photo taken looking up from the casting floor. On the outside you can see plate cooler covers and at the far up top inside, you see two openings where plate coolers were removed.

The cohesive zone shows distinct layers of ore and coke, with the ore semi-molten (light colour) and 'coke windows' clear. Not seen here, but this cohesive zone is similar right around and conical enough – something that is good for BF operation.

As fundamentals do not change, the same phenomena described in Figs 1 and 2 should apply to charcoal blast furnaces.

2.3. Thermal Blast Furnace

Figure 3 is what I call a thermal BF, with heat and temperature distribution along the height of the blast furnace. Temperature distribution is shown in Fig 3(a) in idealized fashion of the many measurements in actual blast furnaces starting in about mid-1960s.

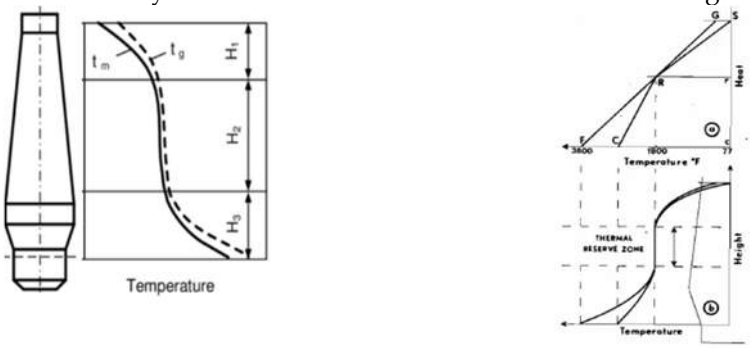

(a) Temperatures (b) Heats.

Figure 3. BF Thermal behaviour

Interestingly, theory on this was developed by BI Kitaev in USSR in early 1950, but being in the Russian language was not available in the West until much later.

In fact, the work assembled in his book was considered so important that the book was translated and edited by Professor PA Young with the title "Heat Exchange in Shaft Furnaces" [8].

In Fig 3(b) the upper diagram is the often forgotten 'Reichardt Diagram' of 1927. Yet, it was the first scientific diagram: 1) describing heating of the cold solids charged at the top of the blast furnace by the gas generated at its flame temperature at the tuyeres and 2) provide heat required by the exothermic reactions of reduction of iron oxides and the endothermic coke gasification.

These fundamental principles will also be fundamental for charcoal.

2 .4. Chemical Blast Furnace

Figure 4 is what I call a chemical BF where chemistry is followed.

As shown in Fig 4, there is a chemically 'Coke Inert Region' and a chemically 'Coke Reactive Region'. The boundary between these two regions is theoretically governed by the thermodynamic equilibrium of Carbon and Oxygen. These are simply stated as:

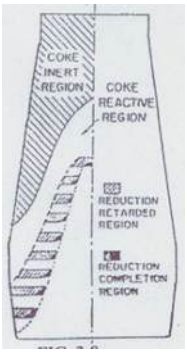

Figure 4. Chemical BF

$$C + O_2 = CO_2 \quad (1)$$

Which is, of course, the combustion reaction and produces heat and high temperature. But thermodynamically CO_2 is unstable at high temperature, so it immediately reacts with carbon as:

$$C + CO_2 = 2CO \quad (2)$$

Incidentally, this is the only oxide reaction that increases entropy [one mole of reactant gas (CO_2) produces two moles of product gas (CO)], so clearly seen in Free Energy Diagrams (Ellingham diagrams) as the only line that slopes down among all others that go up.

Equation (2) is the well-known endothermic Boudouard equation. Its reverse is the Bell's "soot-forming" equation well-known and proven in fire place chimneys.

Although it was stated above that the boundary between the two regions in Fig 4 is theoretically governed by the thermodynamic equilibrium of eqn (2), in real life blast furnace practice chemical kinetics, or rates of reactions, take precedent and carbon reactivity dominates.

Using simple word equation we have the rate for our eqn (2) as:

$$\text{Formation of CO} = \text{Rate Constant x Driving Force} \quad (3)$$

Since the driving force, i.e. concentration of CO_2 in the gas at the same levels in the shaft are same the production of CO by eqn (2) depends only on rate constant, which for carbons is called 'reactivity'.

As ordinary charcoals are more reactive than ordinary cokes is the reason to see in technical literature statements like "Charcoal in BFs is thermally favourable for indirect reduction owing to its higher reactivity" or ""Charcoal has a higher reactivity than coke and reduces the reserve zone temperature which improves efficiency".

It should be noted that without also stating restrictions, statements like this are highly inaccurate and should not be made. The reason is that without at the same time referring to the ferrous burden's reducibility makes the above statements worthless.

Next we consider the "Coke Reactive Region" which from above means that eqn (2) is kinetically favourable and takes place as soon as a CO_2 appears from reduction of FeO forming 2CO by contact with carbon (coke).

For most efficient BF operation we would like to see all of the ore reduced to Fe before melting. There are good reasons for that – the most practical of all is summarised as:

"Blast Furnace Has Never Had Any Problems Melting Iron".

This was clearly demonstrated first time back in 1970 when Jack Peart and Frank Pearce of Stelco charged some DRI from their new SLRN (Stelco Lurgi Republic National) kiln into their BF. The result was, to quote 'It was like the furnace had diarrhoea – we couldn't get the torpedo cars in fast enough to take the metal out'.

As a reminder of what is involved in getting the ore reduced to Fe we look in the previous paper [1] to see that reduction of Hematite to Iron proceeds in steps, ie

$$Fe_2O_3 \rightarrow Fe_3O_4 \rightarrow FeO \rightarrow Fe \quad (4)$$

This is illustrated in Fig 5 for early stage of the reduction which shows that the reduction proceeds topochemically, or onion-like to use every day expression.

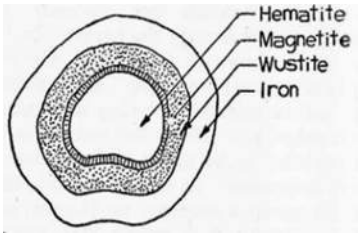

Figure 5. Iron ore reduction

There are only two reductants that thermodynamics tells us can take the oxygen away from the iron oxides. They are CO and H_2.

In the first case the product is CO_2 that is the problem GHG gas and in the second case it is H_2O. As is well known, for centuries it was the CO produced from coke in the blast furnaces that reduced Fe_2O_3 to Fe (iron) in Fig. 5. The BF way of iron ore reduction has been the mainstay of quantity iron production and is still the economically unrivalled process of world-wide iron and steel making industry, but as shown in the previous paper [1], DRI processes are beginning to be considered.

In the end stage of reduction, as indicated in Fig 6, only the FeO is left inside surrounded by Fe metal.

The reaction is then: $FeO + CO = Fe + CO_2$ (5)

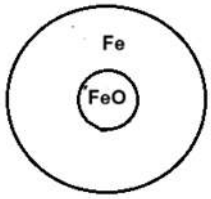

Figure 6. Near end reduction

In following this reaction, we see that the CO molecules have to diffuse through longer and longer distance through the increasing iron layer to reach the FeO. There, the CO reacts with FeO to form Fe and CO_2 molecules which have to diffuse out counter to CO molecules coming in, through longer and longer distance of the iron layer and interfering with CO molecules moving in to react with the remaining FeO, to finally reach the outside and join the upflowing gas.

Time taken to do this, τ, gets longer and longer to convert the last of the FeO to Fe. The equation is:

$$\tau = \frac{\rho R^2}{6bD_eC_g} \quad (6)$$

Where: ϱ - the density of solid reactant, R - is the particle radius, b - the stoichiometric coefficient, Cg - the concentration of the gaseous reactant in the main body of fluid, and De - the diffusion coefficient

Once FeO and CO make contact chemical reaction takes place with the rate given as a simple:

$$r = kCg \quad (7)$$

where k is the rate constant.

Both De and k are temperature dependent so that increased temperatures help kinetics. Unlike in DRI practice [1] where if higher temperatures lead to sticking or swelling, temperatures are adjusted lower to avoid it. In BF practice this is not possible and any stuck together agglomerates will just continue moving down.

This why in practice there is always FeO left inside ore particles before melting zone is reached and provided the amounts are small there is no problem.

Consequences of the ore particles not being well reduced by the time the cohesive zone is reached should be kept in mind. .

1).What happens is that the remaining FeO melts (MP = 1420°C), the liquid FeO immediately contacts the hot CO and immediately reacts, viz. FeO + CO = Fe + CO_2.

2).This Fe having a higher melting point (MP = 1535°C) immediately solidifies and simultaneously the thermodynamically unstable CO_2 just formed reacts with C, viz. CO_2 + C = 2CO – the most endothermic reaction in the BF and takes the heat from the system, and instead of the just formed solid Fe remelting it freezes and, even some just molten FeO freezes too.

3). Of course, the blast furnace has big inertia and can deal with such situations, but too much retained FeO will definitely cause irregularities and increase hot metal costs and is to be avoided.

And being fundamental all of this will also be fundamental for charcoal.

2.5. Blast Furnace Permeability

At this time, it is important to consider the fact seen in Figs 2-4 that a BF has a cohesive zone with 'coke windows' so essential for getting the hot gases made in the raceways to travel up to heat and reduce the iron oxides to Fe metal. Naturally, 'coke windows' must be clear and free of any inclusions that would reduce its flow area. To reach the BF top and do heating and reducing work efficiently the solids in the shaft must have good permeability for these gases.

In practice permeability in blast furnaces has generally meant pressure loss and invariably calculated using Ergun's equation consisting of viscous and kinetic pressure losses, as shown in equation (8) where the terms have their usual meaning.

$$\Delta P_f = 150\ (1-\varepsilon)^2/\varepsilon^3 \times \mu v L_s)/\phi d_p\ + 1.75\ (1-\varepsilon)/\varepsilon^3 \times (\rho L v_s^2)/\phi d_p \qquad (8)$$

The particle size term (ϕd_p) is a reminder that particle shape (ϕ) has an effect on ΔP_f.

Because only the kinetic term is important in blast furnaces the equation used is eq (9) below:

$$\Delta P_f = 1.75\ (1-\varepsilon)/\varepsilon^3 \times (\rho L v_s^2)/(\phi d_p) \qquad (9)$$

I like to define permeability in a more useful way and focussing on the packing rather than the gas, so I say, "Permeability is the ability of a packing to pass gas through it" and so that we can compare permeability of packings, add "under standard conditions of ΔP = 1 atm, A = 1 m^2, L = 1 m and ϱ = air @ STP. So, our equation of permeability, Q cum/s, is then:

$$Q = K\ [(\phi d_p)\ \varepsilon^3\ (1-\varepsilon)\ \psi]^{1/2} \qquad (10)$$

where ψ is a new term called geometric factor with values 0 – 1. The simplest way to look at ψ is to think of a vertical tube filled with packing and air flowing from the bottom. If air flows up unhindered and out freely ψ = 1. If you close the top of tube air flow stops completely and ψ = 0. For other extents of flow hindering ψ = 0 – 1.

It is noted that ΔPf in eq (9) is for normal flow pressures. However, if the pressures are reasonably high, as in modern blast furnaces, then the flow is sufficiently compressible for the driving force to be expressed as:

$$\Delta P_f = [(P_2)^2 - (P_1)^2] \qquad (11)$$

Of course, this does not change the permeability of the system defined in eqn (10).

Recalling the finding of quenched blast furnaces of the greatest importance is that layers of ore and coke set at the stockline do not mix but remain as layers right to the bottom, we note the existence of ore-coke interfaces and explain that for blast furnace ore and coke layers there is an interface every time small size ore is layered on top of the large particle size coke layer and that there is no interface when coke layer is on top of the ore layer. So, for coke on top of ore ψ = 0 and for ore on top of coke ψ > 0.

It is important to be reminded that these interfaces are fundamental result of granular materials' theory of particle segregation with size difference predominating over density and shape. It may be useful to quote a simple segregation rule [9], namely:

For size segregation to occur two requirements must be met simultaneously- there must exist:

1. difference in particle size, and
2. relative motion between particles.

From which clearly: .

ELIMINATE EITHER ONE and YOU ELIMINATE SEGREGATION.

Details of quantifying the value of ψ from particle sizes have been available in blast furnace literature for 50 years [10], so it seems unusual that Ergun's equation [eq (8)] is still widely used instead of eq (10) which represents reality better. It should be remarked that a few papers exist which do discuss, or rather, introduce 'interfaces' as something that could increase furnace pressure drop.

Our 1975 work in Wollongong on ore/coke interface [11] is foundational and seems to be more often used indirectly via subsequent literature rather than explicitly. For example, Propster and Szekely [12] reported laboratory results with layers of different particles and concluded that for small on large conditions the interfacial regions will contribute appreciably to the overall flow resistance.

More recently, Song [13] used cold model experiments with multilayer burden that revealed the pressure drop occurred the most at the layer interface. To find out why he used glass balls and coke particles and showed that the porosity decreased at the interface as the glass balls filled the space between the large sized coke particles. He also found that nut coke mixing ratios of 20 and/or 30% were good for furnace permeability.

These findings are based on experiments done at cold condition (room temperature) only. In blast furnace the burden starts its travels from stockline at the top with ore and coke layers in the throat ending in the bottom part, encountering various physicochemical gas-solid reactions at high temperature in between, plus the reduced ore melting in the cohesive zone area.

All investigations and reports on the effect of ore-coke interfaces on BF permeability in the literature have been done either experimentally on a small scale or with mathematical modelling on industrial scale furnaces.

An exception was when in 1978 I was asked to suggest a design for a simple way to measure BF burden permeability that a real O/C interface was obtained. Figures 7(a) - (c) show this and the results of measurements on a real undisturbed sample from the stockline of a full size rig of Port Kembla No 5 BF built for operators to practice Paul Wurth BLT charging.

It is very important to state that the sample of the full ore layer on coke with an O/C interface in Fig 7(b) was taken from the actual full scale PK BF No 5 stockline after it was layered down by the PW BLT without any disturbance of the particles as they were in that position at the stockline and all subsequent measurements of its size consist and pressures, with actual measurements in Fig 7(c) did not involve disturbances of any kind!

It is also necessary to state that under actual operating conditions the burden is charged against an upcoming hot gas so the very fine ore particles would be elutriated and report in the dust catchers. The ore-coke interface, as such, would still be clearly identifiable and more so in high top pressure blast furnaces.

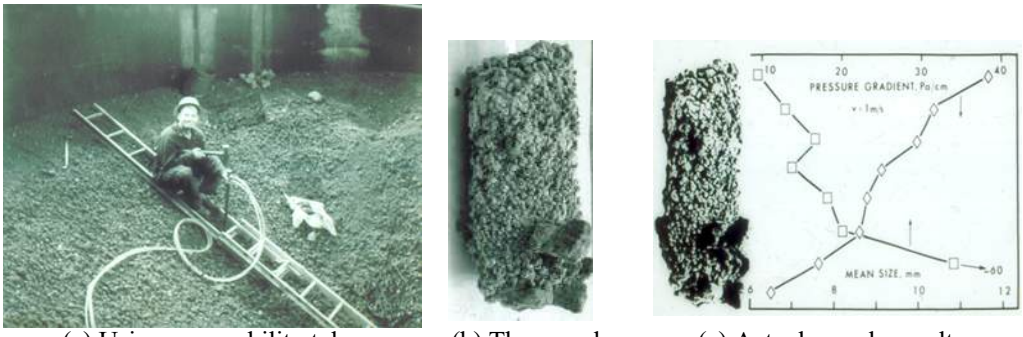

(a) Using permeability tube. (b) The sample. (c) Actual sample results.

Figure 7. Measuring permeability down ore layer at PK No 5 SL and its particle size distribution and pressures on an undisturbed sample withdrawn from the SL shown.

The outer surface of the sample in Fig 7(b) already tells the story starting with layer angle, then of larger particles of sinter with some pellets here and there, then smaller particles above and within the upper part of the coke layer. It is noted that coke sizing specification used in the burden was 25 – 60 mm with 5% max of +60 mm, but it is obvious that a few were really well above 60 mm!

The measurements of actual mean size and pressure gradient of the ore in the sample in Fig 7(c), without disturbing the sample in any way, show ore mean particle size of 12 mm at the top surface decreasing to 6.5 mm at the bottom. The pressure gradient starts at 10 Pa/cm at the top, with a gradual increase to 20 Pa/cm for about 2/3 of the height and then in the last 1/3 - which can be seen to be an interface a huge 60 Pa/cm.

Saying this in another way is that the gas flow in one third of an ore layer experiences resistance three times higher than its resistance in the rest two thirds of it!

3. APPLICATION TO LARGE BF TO USE CHARCOAL BURDEN

3.1. Preliminaries

As noted earlier, most papers on charcoal in large blast furnaces deal with charcoal injection. The reason is to save the expensive coke – and the injection rates spoken of are in 200-300 kg/thm by weight.

This paper considers replacing major part (300kg/thm) of the carbon of BF burden with charcoal, not a small part (20kg/thm) reported to have been tried with good results [21,22], nor as additions to coking blends [23]. In this respect replacing major part of the carbon of BF burden with charcoal appears to be presented here for the first time in the blast furnace industry.

Preceding material established unambiguously that small BFs in Iron and Steel industry, especially in Brazil, have been successfully operating in practice with 100% charcoal for many years. Likewise, an exhaustive search of literature carried out at the same time showed that apart for recent interest in substituting some of the currently used injectants, like pulverised coal, with charcoal, there have been no publications of using 100% charcoal in the burden of large (>2000cum) blast furnaces.

The material presented here in previous chapters also showed that theory of iron making in any type of reactor follows the same rules of chemistry, thermodynamics, kinetics, fluid flow, engineering and reactants contacting, be it Midrex, Hylsa, ZESTY, etc

for making of solid iron, or with melting to make pig iron in coke and charcoal blast furnaces.

In summary – and an important one that should be highlighted and kept in mind is:

The two zones, i.e. 'coke inert zone' and 'coke reactive zone'
are the product of Boudouard reaction rates – NOT equilibrium,
so their rate constants can be changed.

3.2. Bringing Everything Together

To sum up so far. AFOLU emissions released by lands and forests in Indonesia produce twice as much greenhouse gases than other emissions and reducing them via charcoal in making iron and steel gives twice the benefit and even more with using charcoal to reform CO_2 produced.

As was demonstrated in the recent paper [1], reducing CO_2 can be done with DRI production immediately and assisted by hydrogen if it is economic. However, there are many operating high capital cost iron blast furnaces in Indonesia and worldwide using coke, so economically this means that most blast furnaces with their coke ovens will continue producing iron and large amounts of GHG emissions.

As charcoal is CO_2 neutral – and is also carbon - can it substitute coke in the coke iron blast furnace?

To answer it, we need to establish if coke can technically be substituted by charcoal and whether it can be done by a full substitution as in Brazil or not, and how economic is it likely to be.

It has been demonstrated in this paper so far that small charcoal blast furnaces have been producing iron for decades – and more importantly that their internal state, including the cohesive zone, are similar to coke blast furnaces.

It is true that the larger is the coke blast furnace the better quality its coke must be and by analogy the same must apply to large charcoal blast furnaces. And here it must be stressed that the science has moved on, and our views should too.

What this means is that charcoals (biochars) can now me made with properties that are not too different from coke. In fact, there have been companies very recently in many countries who have developed charcoal making processes of 'metallurgical charcoal'. One was mentioned in the previous paper [1] as the CSIRO 'Metallurgical Charcoal', others are 'Pyrochar' claimed to be 'replacement to coal in primary metals manufacture' [14], and especially 'BioCarbon' [15] that has developed charcoal based, coke replacement products

for EAF steelmaking and ferroalloy production, and said to be working towards achieving properties approaching BF coke.

With all the facts, evidence and theory presented above backing us we can confidently consider the following proposal.

We have a large BF in a steel plant. The BF produces 4,000,000 thm/year. As its burden we intend to use:

1. imported iron ore pellets (6-20mm),
2. a fixed amount of 125 kg/thm of coke made in the plant's coke ovens (20-50mm), and
3. 300 kg/thm of charcoal having similar properties to the coke (20-50mm).

Air is preheated to 1200°C in hot blast stoves with BFG and COG. To balance the BF's energy, carbonaceous material, including charcoal fines, are tuyere injected.

Energy-wise the products BFG and COG at 18.0 PJ/year and 3.0 PJ/year is sufficient to heat the coke ovens themselves and hot blast stoves for 8.6x106 m3/year blast at 1200°C and 2.5 atm(abs).

Cost-wise the answer is simple. We are substituting the same amount of cheaper charcoal with 2% ash for the more expensive coke and its 14% ash, so it will not be surprising if the costs are lower!

For this blast furnace operation, as can be seen, we are using two different carbons, namely: 1) the cohesive zone part and 2) the shaft zone part. This appears to be the first time that this has been done, as so far these two quite different evidence-based theory requirements of a blast furnace carbon have been invariably introduced as a single carbon, namely: coke in coke BFs and charcoal in charcoal BFs.

The coke comprising the 125 kg/thm of "cohesive zone coke" would be strong, unreactive and shatterproof – not unlike the "cupola coke" which is just like that. The cohesive zone coke will be added with the 300 kg/thm of charcoal and layer charged. In moving down, this layer will first be contacted by the upcoming hot gas to be heated to reserve zone temperature. As both coke and charcoal have similar effective thermal conductivities, reaching uniform temperature will be no different for the various sizes to what it is now.

In the reserve zone the CO_2 product of iron ore reduction will be mostly reacted with the more reactive charcoal than with essentially unreactive coke. This is simply a consequence of a higher reactivity of charcoal compared with coke in the word equation for reaction rate shown in eqn (3), viz:

$$\text{Formation of CO} = \text{Rate Constant x Driving Force}$$

Since the driving force, i.e. concentration of CO_2 in the gas is the same at the same level in the shaft, the regeneration rate of CO_2 by gasification of carbon, or $CO_2 + C = 2CO$ depends only on rate constant, or reactivity.

This is absolutely expected from theory. The finding by the Aachen team mentioned earlier "that coke reactivity in CO_2 atmosphere decreases when charcoal particles are attached on the coke surface, which evidently protects coke from the solution loss

reaction." is therefore unsurprising. Nevertheless, it is important because it is a practical BF confirmation of using both carbonaceous materials at the same time, as proposed here.

As to the best particle sizes chemistry and permeability counter each other. Chemistry says small size – permeability says large size. This means we need to find the best compromise.

3.2.1. Chemistry says small size

As shown earlier in eqn (4), the reduction of Hematite to Iron proceeds in steps, ie

$$Fe_2O_3 \rightarrow Fe_3O_4 \rightarrow FeO \rightarrow Fe$$

This was illustrated in Fig 5 for early stage of the reduction which shows that the reduction proceeds topochemically, or onion-like to use an everyday expression, and in Fig 6, for near the end of reduction when only FeO is left inside surrounded by Fe metal.

It was also shown that because of diffusion of CO from outside gas through the Fe shell to reach the FeO, react according to eqn (5), namely $FeO + CO = Fe + CO_2$ and the product CO_2 to diffuse back through the Fe shell to finally reach the outside gas is a very difficult task.

An additional benefit of using hydrogen, besides its product being a friendly H_2O, is that both H_2 and H_2O molecules are much smaller than both CO and CO_2 and increase the reduction rate significantly.

Actually, as discussed earlier, it is again pointed out that any increase in reduction rate means an increase in the diffusion coefficient, to get the reactants together quicker to get benefits of high reaction rate coefficient.

It was also pointed out earlier that with the best will in the world, in actual blast furnace practice – and in DRI practice, too – there will always be FeO left inside ore particles before melting zone is reached and provided the amounts are small there is no problem.

To end this part of chemistry and particle size it is worth repeating the consequences of the ore particles not being well reduced by the time the cohesive zone is reached, namely: .

1). The remaining FeO melts (MP = 1420^{o}C), the liquid FeO immediately contacts the hot CO and immediately reacts, viz. $FeO + CO = Fe + CO_2$. .

2). This Fe having a higher melting point (MP = 1535^{o}C) immediately solidifies and simultaneously the thermodynamically unstable CO_2 just formed, reacts with C, viz. $CO_2 + C = 2CO$ – the most endothermic reaction in the BF, and takes the heat from the system, and instead of the just formed solid Fe remelting it freezes and, even some just molten FeO freezes too.

3). Of course, the blast furnace has big inertia and can deal with such situations, but too much retained FeO will definitely cause irregularities and increase hot metal costs and is to be avoided.

The answer to this dilemma of reducibility of ferrous part of the burden is to design pellets with high reducibilty while keeping their strength properties the same. This idea is not new, and many ways have been tried, from adding saw dust to pellets to making iron carbon composites ("Ferrocoke") by adding coke particles to ore [16], and so on.

However, for some reason none of these ideas have been implemented 'en masse' as a standard procedure.

As the science has moved on fast in the last few years, it is quite likely that an economic and a practical method will be found to increase reducibility of pellets, which may well involve use of catalysts.

And being fundamental all of this will also be fundamental for charcoal.

3.2.2. Permeability says large size

Now we consider the other half of the compromise, namely particle size and permeability.

Theory and its useful practical equation, incorporating a new term, ψ, called an interface factor, was presented earlier in eqn (10).

Note in eqn (10) the huge importance of bed porosity (ε), also known as voidage, compared with d_p, the particle size. For example, for a bed porosity of 0.5, the effect is $[\varepsilon^3 (1- \varepsilon)]^{1/2} = [0.5^3 (1-0.5)]^{1/2} = [0.5^4]^{1/2} = 0.5^2$, whilst for particle size its effect on permeability is only $(d_p)^{1/2}$.

As an example, consider the porosity or voidage (ε), of various mixtures of three ore sizes, namely: 7mm, 14mm and 28mm. The measured porosities, plotted on the ternary diagram in Fig. 8, so that any point inside the triangle is a mixture of these three size ores, show a map of 'isopores', ie lines of mixtures of these three sizes of ore that have the same porosity.

This is the same interpretation as that of a daily weather map of isobars.

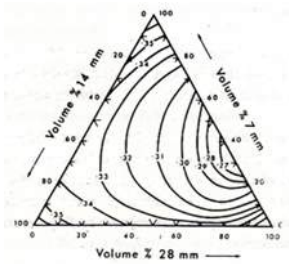

Figure 8. Ternary porosities

To explain further: each corner corresponds to 100% of each of the three sizes, with the side opposite being 0%. Each side therefore corresponds to a mixture of two sizes. For example, the bottom side of the triangle in Fig 8 corresponds to mixtures of 14mm and 28mm – no 7mm!

If we now draw, say, 10 lines parallel to the bottom side of the triangle going up to the top corner of 100% 7mm ore, each of these lines will correspond to 10% of the 7mm ore, first line up is 10%, next line up is 20%, and so on – each time the other two sizes are the difference from 100%. The point in the middle of the triangle is a mixture of 1/3rd, 1/3rd and 1/3rd, or 33.3% 7mm, 33.3% 14mm and 33.3% 28mm – of course!

It can be seen that he lowest porosity in this three sizes ore mixtures in Fig. 8, occurs in a binary mixture of 28mm particles and 7mm particles at $\varepsilon = 0.26$. Although to many people this may seem strange, it is expected from granular materials theory. In other

words, no matter how many different size particles a mixture has, the minimum porosity would always be in a binary mixture of the largest and the smallest particles and always at around 30% of the smallest size particles.

Figure 9 shows permeabilities of mixtures of three sizes, for generality labelled L, M and S, or Large, Medium and Small. Being a ternary system, each corner is 100% and everything else explained before for Fig 8 is the same, except, of course, that the lines inside are lines of equal permeabilities or "isoperms" calculated by eqn (10). In this case, for simplicity the permeability (Q) of beds of large particles at the 100% L corner is the highest (Q =10), reducing to Q = 1 for beds of small particles at the 100% S at the top corner.

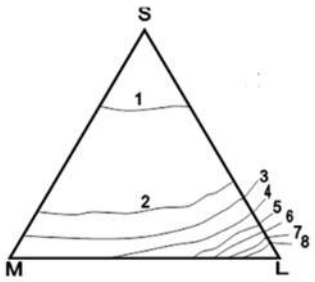

Figure 9. Ternary permeabilities

It is quite clear from Fig 9 that the highest permeabilities are at the large size corner (L) – then the permeability decreases very, very rapidly around the L corner and then remains essentially low for the rest of the other 85% of mixtures.

In view of the crowding of isopores at the largest particle size corner in Fig 8, we can say that the crowding of isoperms at the largest particle size corner L, in Fig 9, should not be unexpected.

As a result of this we can formulate a Permeability Rule, namely:

For high permeabilies do not mix small size particles with large particles but keep them away from each other as much as possible.

Apart from its critical role of providing permeability for hot gases to travel from the bottom to the top of the BF, coke in blast furnaces also serves a number of fundamental purposes.

They are, in round figures: 1) Heat source - 60%, 2) Reducing agent - 30% and 3) Carburising agent - 10%.

To complete our task of finding best particle size compromise we need to take up the behaviour of carbon particles in the cohesive zone, deadman and the hearth to maintain good permeability for gases and liquids (iron and slag) and to carburize iron before it is cast.

Fortunately, there have been recent papers on dissection results of these zones in large blast furnaces, 2200 m3 [17] and 2800 m3 and 5500 m3[18], all in PRC.

The dissections found that total region porosity of deadman was 0.3 with centre of 0.25. Therefore, improving the porosity of the central deadman is important to make the high temperature tuyere gas reach the centre zone of the hearth. With large blast furnaces hearth diameters are large, too, 15m for the 5500 m^3 one, so with raceways depths of

around 1.5m, the hot gas has to travel about 6m through a coke bed to reach the centre. This also explains the observed lower molten iron velocity in the centre compared with its higher velocity near the side wall

Porosities of ore and coke layers in the shaft of a BF are typically 0.4 and 0.5, and M40 for big BF must be +80% and M10 must be -6%.

Other parameters of BF burdens are:

Ore – Size: 6-20mm. Strength: -3.15mm 2%max. Swelling Index: 13-18%. Reducibility: 65%.

Coke – Size: 25-80mm. Strength: M40 >85%, M10 <7%. CSR >65%. CRI <25%.

In the dissected 2200 cum BF[17] the average voidage of the deadman in the hearth was 41.1%, the mean size of the charged coke was 54.9 mm and that of the dissected hearth was 34.5mm in the centre and gradually decreased to 27.6 mm at the wall. Also, the closer to the bottom of the hearth vertically, the smaller the coke size was from 34.6mm to 27.8mm, or almost identical variation as horizontally.

The M40 of hearth coke was observed to have decreased by about 13% compared with feed coke, and M10 had increased by 63% compared with the coke in the upper part.

For the 2,800cum BF[18], deadman coke was 28.2mm centre, and 25.4mm at the wall. The M10 and M40 of the feed coke was 88% and 6%, respectively. Compared with feed coke, the M40 of hearth coke was observed to decrease by about 13% and the M10 increased by 144%. The M10 increased with the increasing distance to the tuyere level while the M40 decreased with the distance.

In the 5,500cum BF[18], the average porosity of the deadman coke at the edge, the middle and the centre areas was 0.33, 0.30 and 0.25, respectively. Hearth coke average M10 was 14% and M40 was 77%.

So, for these large blast furnaces, the reduction of coke size and its strength from the stockline to the hearth was something normal and expected. However, as the dissection results showed, the reduction in both were mild, except for M10 which was high, and also expected – and the reason is the number 3) of coke's fundamental purposes listed earlier, namely: carburizing agent.

As a reminder, carburization in the hearth occurs primarily via:

$$Fe(liq) + C(solid) \rightarrow Fe\text{-}C(liq) \qquad (11)$$

and is endothermic under blast furnace conditions, meaning it absorbs heat. The enthalpy change (ΔH) depends on the form of carbon. In any case it is small 0.4-0.6 GJ/t, compared with the huge total BF heat flow of 13-15GJ/thm, and as noted before, the blast furnace has a large thermal inertia and can readily deal with it.

The rate of carburisation, eqn.(11), depends on: (i) carbon activity difference between molten iron and the solid carbon source - and charcoal being more active than coke, would show higher rates - and (ii) surface area. And as small size particles have a large area/unit

weight explains why M10 of the coke in dissected hearth of BFs referred to above, was high.

It is also important to note that theory shows that, on average, granular particles contain the same number of internal cracks or defects per unit volume.

A. Specifying large size feed coke for blast furnaces, believing that it will not break up on the way to the hearth and decrease voidage, is something entrenched hard in the ironmaking industry.
B. The other belief that the voidage of large size particles is always greater than that of the small size particles is one of the most deeply entrenched misconception in practice. The reason is mistaking void size and void volume – the two are quite different concept.

Therefore, all the evidence-based results, presented in this paper support the proposal for BF burdens to consist of a ferrous part and two carbon parts, namely:

1. coke for the cohesive zone and hearth and
2. charcoal for heating and reduction.

The ferrous part can be pellets or sinter with appropriate physical and chemical properties and a reducibility to match the charcoal's reactivity. The size range of these should be governed by how high a reducibility can be achieved on a continuous basis.

The carbonaceous part will be: 1 - Unreactive coke of cupola quality in the size range 20 – 50 mm and, 2 - Charcoal compacts, of similar physical and chemical properties to coke ovens coke and a reactivity to match the ferrous part's reducibility. The size range of this charcoal should also be 20 – 50 mm.

It is expected that the cohesive zone structure and the deadman and their performance would not be too different from those now. However, the burden being lighter because for the same carbon content a 10-12% lower ash in charcoal would make the buoyancy force of the liquid metal in the hearth greater and lead to a higher coke-free layer at the bottom.

This could actually have a positive effect as recently reported by Wang et al [20] that "maintaining a higher floating height of the deadman is more beneficial for the overall protection of the hearth".

Finally, for our 4,000cum BF example the CO_2/thm in the top gas is 265 kg from charcoal and about 140 kg from coke and injectants and this 140kg of CO_2 can be converted to CO in charcoal gasifiers (see [1]) to make the BF be a true "green BF".

4. SCOPE LIMITATIONS AND FUTURE WORK

4.1. Scope of the Present Study

The present work presents what is almost certain the first to document a "dual-carbon " blast furnace burden combining two carbons 'cohesive zone' coke portion and a larger share of dense charcoal 'stack' portion. This assignment of carbons recognises distinct functional roles of carbons within the furnace that have been traditionally served by one – coke in coke BFs and charcoal in charcoal BFs. The study is backed by both blast furnace up-to-date theory and practice and a focus is on metallurgical compatibility with established blast furnace constraints.

The study can not – and does not - demonstrate operational maturity, extended campaign performance, or site-specific optimisation. What it does demonstrate is that the proposed configuration is physically aligned within known blast furnace theory and operating envelopes, thereby justifying further investigation for optimisation.

With all the ironmaking industry facts, evidence and theory presented here backing us we can confidently say that a dual-carbon blast furnace will work. On the other hand with Paul Wurth/SMS syngas stack injection of EASyMelt [24] process for which theory and the 1970 ironmaking industry facts of Hirohata No 4 BF do not back it, we can confidently say that it will not work!

4.2. Limitations

Several limitations consistent with every new concept are acknowledged.

- Technology Readiness Level (TRL):
The concept corresponds to an early TRL, in that it has never been done, as such, though all the individual parts have been done and it is already known what would happen . This is why it is recommended to do it in an actual blast furnace.

- Materials Behaviour:
While the functional use and properties of conventional coke and conventional charcoal in blast furnaces are historically established, their behaviour can not be currently predicted with any precision and is still managed empirically in practice. Actually, the coke in this dual-carbon charge is 'cupola coke'used in foundries for 100 years, so much is known about it.

-

Cohesive Zone and Campaign Behaviour:
Cohesive zone geometry can only be determined by quenching and excavation. In operation its geometry and stability are inferred operationally or mathematically, rather than directly. Its extended campaign behaviour of the dual-carbon configuration therefore cannot be unambigously demonstrated within the scope of this work.

- Energy Balance Quantification
Although enhanced endothermicity of conventional charcoal due to its increased reactivity is well known, that of compacted charcoal of the dual-carbon charge of this operation is unknown, but expected to be not too different from that of normal BF coke. As such analysis would require campaign-specific operating data it is beyond the scope of conceptual study.

- Economics and Supply Chain
The paper does not present a detailed techno-economic assessment or a comprehensive biomass supply-chain analysis. Statements regarding potential cost advantage are intended as first-order indications rather than quantified economic claim.

These limitations are explicitly recognised to ensure clarity regarding the scope and intent of the study.

4.3. Future Work and Development Pathway

The results of the present study define a clear pathway for future improvements, research and development.

4.3.1. Subsystem-Level Experimental Validation

- Dense charcoal reactivity and attrition testing.
- Gasification behaviour above the cohesive zone.
- Raceway and hearth heat balance sensitivity to carbon distribution.

4.3.2. Process Modelling and energy Balance Closure

Development of a zone-based furnace model to enable:

- Quantification of thermal redistribution effects.
- Evaluation of thermal load vs control variables.
- Sensitivity analysis of thermal resilience under operating conditions.

4.3.3. Operational Monitoring and Control Studies.

Integration of the dual-carbon concept into existing BF control framework could be explored using:

- Top gas composition and pressure drop data.
- Burden distribution and descent.
- Dynamic response analysis to blast and burden fluctuation.

4.3.4. Techno-Economic and Sustainability Assessment.

A full techno-economic assessment, incorporating dense charcoal and cupola quality coke – production, logistics, handling infrastructure and maintenance impacts on additional - and reduced equipment, should be conducted on a site-specific basis. In parallel, regonal sustainability assessment addressing land use, governance and supply-chain resilience are required to inform responsible deployment.

4.4. Concluding Note.

The dual-carbon blast furnace concept presented here for the first time can not be proposed as a fully developed turn-key industrial solution to 'green blast furnace', but as 100% technically and practically supported actual operating parts making up the whole coherent framework that aligns with established blast furnace theory while enabling substantial reduction in fossil carbon dependence. The identified limitations are only those of scale and not of substance and define investigation priorities for optimisation rather than feasibility barriers and provide a structured basis for advancing the concept toward implementation to operating level of technological readiness.

5. CONCLUSIONS AND RECOMMENDATIONS

5.1. Conclusions

There are many operating iron blast furnaces in Indonesia and worldwide using coke and being capital intensive they must be operated for a long time. This means that most blast furnaces, nowadays large, with their coke ovens will continue producing iron and large amounts of CO_2 for many years yet, making zero carbon unattainable.

It was shown in the recent paper in this journal [1] that sponge iron can be produced in large 2.5 mty DRI reactors using charcoal and that making charcoal using tree plantations and no automation would give employment to millions of Indonesian workers.

AFOLU (Agriculture, Forestry and Other Land Use), emissions released by lands and forests in Indonesia produce twice as much greenhouse gases than other emissions [2, 3] and reducing them via charcoal, particularly in making iron and steel gives twice the benefit.

In October 2025, President Prabowo announced full support for Brazil's TFFF (Tropical Forest Forever Facility) by stating: "Brazil pioneered this movement to save forests, and we will commit whatever amount Brazil has invested there - Indonesia will invest here."

All government laws and regulations already exist and this paper gives strong technical evidence that a dual-carbon BF operation will work. It specifically demonstrates, almost certainly for the first time, that there are two fundamentally different carbons in blast furnaces namely: the cohesive zone carbon and the shaft zone carbon.

It is also demonstrated that large blast furnaces can operate with this dual-carbon burden not too differently from a 100% coke or a 100% charcoal carbon burdens.

Clearly, this can be viewed as good economics as we are simply substituting the same amount of cheaper charcoal carbon for the more expensive coke carbon.

5.2. Recommendations

Because ironmakers are naturally cautious of any new changes in operation and overly traditional in their thinking, it is recommended that a test of the proposed dual-carbon burden be made directly in a medium size coke blast furnace (≈1,000cum) with a stepwise replacement of coke with dual-carbon quality charcoal.

The reason for not starting with laboratory tests and progressing up in scale is threefold: 1) we already have these laboratory results, 2) we already know their BF shaft reactions, and 3) we need to test dual-carbon burden cohesive zone behaviour which has never been done before and therefore is not available anywhere in the world.

Acknowledgements

I am grateful to Dr Pramusanto who introduced me long ago to the experimental charcoal blast furnace in Lampung and to a taste of Indonesian colourful culture and tradition, so when an opportunity arose to start a UOW Campus in Cilegon and spend many years in Indonesia, I did not hesitate.

References

[1] Nicholas Standish (2025). Climate Change in Indonesia:Green Steel. Recent in Engineering Science and Technology, 3(03), 54–68.
[2] World Resources Institute December 5, 2024.
[3] Ahmad Zaki, UGM Faculty Economy and Business 2022.
[4] Palmoil magazine June 10, 2025 Ermanto Fahamsyah,University of Jember.
[5] Renato Rostas, Brazil at steel decarbonization crossroads: Fastmarkets, March 21, 2022.
[6]. Jose Adilson de Castro, GA Medeiros, EM Oliveira, MF Campos and Hiroshi Nogami (2020). The Mini Blast Furnace Process: An Efficient Reactor for Green Pig Iron Production Using Charcoal and Hydrogen-Rich Gas: A Study of Cases: Metals, 10(11), 1501–23.
[7] A. Babich, D. Senk and M. Fernandez (2010). Charcoal Behaviour by Its Injection into the Modern Blast Furnace. ISIJ International, 50(01), 81–88.
[8] B. I. Kitaev, Y. G. Yaroshenko and V. D. Suchkov: Heat Exchange in Shaft Furnaces. Elsevier, 1976.
[9] N. Standish: Bulk Density of Coal. National Energy Research and Development Program (NERDDP). Wollongong University Press, 1990.
[10] N. Standish, Editor: Proceedings of Blast Furnace Aerodynamics Symposium, AusIMM Press, 1975.
[11] N. Standish, P. W. Boehme and O.R. Gregory (1975). The Ore-Coke Interface: Mixed Ore Results: Proceedings of Blast Furnace Aerodynamics Symposium, AusIMM Press.
[12] M. Propster and J. Szekely (1977). The Porosity of Systems Consisting of Layers of Different Particles: Powder Tech. 17(01), 123-38.
[13] Q. Song (2013). Effect of Nut Coke on the Performance of the Ironmaking Blast Furnace: PhD Thesis, Delft University of Technology, Delft, NL, 1–149.
[14] Pyrochar (Pty) Ltd (2023). Low Emission Charcoal (Carbon) Green Charcoal. Google.

[15] BioCarbon (2023). How Converting Low-value Biomass Can Pave the Way Towards Sustainability: Editorial Team, Green Steel World, October 18.

[16] T. Ariyama , M. Sato, T. Nouchi and K. Takahashi (2016). Evolution of Blast Furnace Process toward Reductant Flexibility and Carbon Dioxide Mitigation in Steel Works: ISIJ International. 56(10), 1681-96.

[17] S. Meng, K. Jiao, J. Zhang, C. Wang, L. Zhang, Z. Guo and Z. Xiao (2023). Analysis of the coke distribution characteristics in hearth based on blast furnace dissection. Fuel Processing Technology. 242,

[18] Q. Niu, S. Cheng, W. Xu, W. Niu and Y. Mei (2019). Analysis of the Coke Particle Size Distribution and Porosity of Deadman Based on Blast Furnace Hearth Dissection. JISI International. 59, (11),1997-2004.

[19] M. Sun, J. Zhang, K. Li, S.Ren, Z. Wang, C.Jiang, and H. Li. (2019). Dissolution Behaviour of Various Carbonaceous Materials in Liquid Iron: Advances in Surface Engineering. 71. 4305-310.

[20] F. Yuan, L. Chen, L. Wang, L. Zhao, and Y. Zhong (2025). Study on the Effect of Deadman State on Blast Furnace Hearth Erosion Based on Solidification and Melting Model. IEEE Access 13, 21811- 826.

[21] A.Hesham (2018). New Trends in the Application of Carbon-Bearing Materials in Blast Furnace Ironmaking. Minerals, 8(12), 561-73.

[22] F. Hanrot, D. Sert, J. Delinchant, R. Pietruck, T. Bürgler, A. Babich, M. Fernández, R. Alvarez and M. Diez (2009). CO2 Mitigation for Steelmaking Using Charcoal and Plastics Wastes as Reducing Agents and Secondary Raw Materials. 1st Spanish National Conference on Advances in Materials Recycling and Eco – Energy Madrid, 12-13 November 2009.

[23] J. MacPhee, J. Gransden, L. Giroux and J. Price (2009). Possible CO_2 mitigation via addition of charcoal to coking coal blends. Fuel Processing Technology, 90, (1),16-20.

[24] P. Kinzel. Turning Metals Green with EASyMelt. SMS Magazine. 14 December. 2023.

RiESTech
Recent in Engineering Science and Technology

MBI

Article

Pipe Stress Analysis of the Steam Pipe of Project Tidore Power Plant (2 X 4 MW) Using CAESAR II

Franky G Pasaribu [1,*], Johny Wahyuadi Mudaryoto [2], and Robert H Pasaribu [3]

[1] Department of Metallurgical and Materials Engineering, Universitas Indonesia, Depok, Indonesia
* Correspondence: frankypasaribu14@gmail.com

Abstract: Pipe stress analysis is an important step to ensure that the piping system can function properly and safely. The main goal is to ensure that the piping design can withstand the pressure and load without failure. Pipe stress analysis is essential because piping systems in power plants are subjected to various loading conditions, including internal pressure, thermal expansion, self-weight, and external forces. Proper analysis helps to prevent excessive deformation, leakage, fatigue, and potential of failured. It also ensures compliance with ASME B31.1 requirements by verifying allowable stresses, flexibility, and support configuration, thereby improving system reliability and operational safety. This analysis follows the guidelines of ASME B31.1 Power Piping, which regulates the design and construction of piping in a Power Plant. The analysis was performed using Caesar II software. This software helps evaluate various working conditions and measure the stresses in the piping system. From the analysis report, no overstress problems were found in the steam piping line. Since the system already meets ASME B31.1 standards, no changes were needed to the number, position, or type of pipe supports.

Keywords: Stress; Load; Overstress; Pipe Support

Citation: Pasaribu, F. G., Mudaryoto J. W., Pasaribu, R.H. (2026). Pipe Stress Analysis of the Steam Pipe of Project Tidore Power Plant (2 X 4 MW) Using CAESAR II. Recent in Engineering Science and Technology, 4(01), 22–37. Retrieved from https://www.mbi-journals.com/index.php/riestech/article/view/129

Academic Editor: Vika Rizkia

Received: 24 September 2025
Accepted: 30 November 2025
Published: 31 January 2026

Publisher's Note: MBI stays neutral with regard to jurisdictional claims in published maps and institutional affiliations.

1. Introduction

The Indonesian government is striving to increase the development of affordable and efficient power generation systems to meet the country's electricity needs. A piping system in a power plant serves a primary function as a transportation pathway for fluid flow, whether gas or liquid, in hot, cold, or pressurized conditions. A piping system is essentially a system for delivering fluid from one location to another to enable subsequent processes.

However, the piping system is complex, and its design must consider many aspects to achieve an effective and efficient system. Stress that occurs in a pipeline is predominantly caused by the design itself. In a pipeline system, branching may occur, which becomes a critical factor that must be carefully considered due to the stress it introduces. By understanding and analyzing the magnitude of stress, it is possible to minimize it to ensure safe operation and extend the lifespan of the piping system [2].

Today, several software tools are available to assist in stress analysis of piping systems. These tools comply with the standard requirements for stress analysis aids, as they are based on established piping codes and standards. Each software has its similarities and differences.

CAESAR II was used, because this software is one of the most widely used pipe stress analysis software in various industries due to its comprehensive analytical capabilities and strong compliance with international standards such as ASME B31.1. The software allows detailed modeling of piping geometry, simulation of operating conditions, and accurate evaluation of stresses, displacements, and support loads. CAESAR II selected in this study because it offers reliable calculation accuracy, an extensive material database, and user-friendly modeling features that support efficient analysis. CAESAR II provides several advantages, including complete stress analysis functions such as thermal, pressure, occasional, and dynamic loads. CAESAR II also provide clear visualization of results, and can integration with 3D design tools.

Based on the background described, the main issues discussed in this study are the stress analysis of the steam line pipe from the superheated boiler to the steam turbine at the existing PLTU Tidore, North Maluku [6].

The analysis is limited to the steam line route from the superheater boiler to the Main Steam Valve and evaluates the efficiency of the pipe support system. This study refers solely to the ASME B31.1 standard. It does not cover topics such as corrosion, corrosion protection systems, pipe installation processes, detailed calculations of stress, forces, and moments, nor does it consider pressure drop, heat loss, friction loss, or the impact of seismic and wind loads. All welded joints are assumed to comply with the ASME BPV Section IX code and standards [1].

The main objective of this study is to conduct piping stress analysis to ensure that the piping system operates safely and complies with the relevant standards, particularly ASME B31.1 [1] [3]. This analysis is essential to minimize the actual loads (forces, moments, and stresses) occurring on the pipe and equipment nozzles, so they remain within the limits set by international codes and standards such as ASME, ANSI, API, WRC, and NEMA [7][8]. This analysis focuses specifically on static loads, and proper support installation plays a vital role in preventing system failures or damage during operation due to static and dynamic loading conditions [11].

The scope of this analysis falls under the ASME B31.1 (Power Piping) standard, which is widely used in industrial applications such as power plants [2][6]. Stress analysis is carried out to ensure that the piping routes, nozzle loads, and support placements are appropriately designed so that the resulting stress does not exceed the maximum limits specified by the standard ASME B31.1[1]. To perform this analysis, piping engineers commonly use specialized software tools such as CAESAR II [4][5].

2. Materials and Experimental Methods

The following data is inputted into the software and obtained from the isometric drawing with line number 8-LB-20116-F1-H100, from the boiler to the main steam valve of the turbine at the Tidore Coal-Fired Power Plant (PLTU Tidore), North Maluku which is the design and operating condition based on **Table 1**.

Table 1. Pipe Design and Operation

Parameters	Value	Unit
Pipe Identification	8-LB-20116-F1-H100	-
Material	ASTM A 335 P11 Ferritic Alloy-Steel	-
Yield Strength	60,190.7	Psi
Tensile Strength	29,732.7	Psi
Design Code	ASME B31.1	-
Pipe Products	Steam	-
Nominal OD	219.1	mm
Thickness	18.26	mm
CA	3.175	Mm
Design Temperature	500	^{0} C
Operating Temperature	490	^{0} C
Design Pressure	8,296.159	Psi
Operating Pressure	7,541.96	Psi
Insulation	Calcium Silicate	
Insulation Thickness	100	mm

A literature study was conducted to obtain relevant information for this final project. The information was gathered from books, journals, PLTU Tidore data, the CAESAR II manual, and various other sources.

In applying design code standards, engineers must understand the basic principles of pipe stress and related concepts. A pipe is considered to have failed if the internal stress exceeds the allowable stress of the material. Stress is a vector quantity, meaning it has both magnitude and direction. The magnitude of stress is defined as force (F) divided by area (A). To define the direction of stress in a pipe, three principal axes are used, arranged perpendicularly as shown in Figure 1.

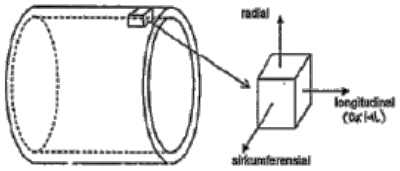

Figure 1. Directional Stress in Piping

Based on this simple definition, two key terms need to be clearly understood: internal stress and allowable stress. Internal stress is caused by external loads such as dead weight, internal pressure, and thermal expansion. It depends on the pipe's geometry and the material used. On the other hand, allowable stress is mainly determined by the material properties and how the pipe is manufactured. These two stress values are compared using failure theories.

When discussing code standards, it is essential to distinguish between the two types of pipe stress:

- Actual pipe stress is obtained by strain gauge measurement or manual/ software-based calculation.
- Code pipe stress, which is calculated using stress formulas defined in a specific code standard.

The axis perpendicular to the pipe wall and pointing outward from the pipe center is called the radial axis. The axis lying along the pipe wall but perpendicular to the longitudinal axis is the tangential or circumferential axis. The longitudinal axis lies in the middle of the pipe wall and runs parallel to the length of the pipe.

2.1 Principle Stresses in Piping

a. Longitudinal Stress (SL)

Longitudinal stress, also called axial stress, acts in the direction parallel to the longitudinal axis of the pipe. This stress is considered positive if compressive (caused by pushing forces). In piping systems, longitudinal stress occurs due to internal pressure forces and bending moments. An illustration of this can be seen in Figure 2.

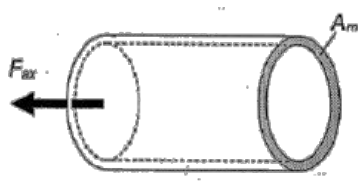

Figure 2. Direction of Pipe Axial Force

$$S_L = \frac{F_{ax}}{A_m}$$

Where:

F_{ax} = internal axial force A_m= cross-sectional area of the pipe material $= \pi d_m t$

d_{md}= mean diameter of the pipe

d_{od} = outer diameter of the pipe

d_{id} = inner diameter of the pipe

b. Effect of Pipe Pressure

For simplicity, this final equation is often written in a conservative form:

$$S_L = \frac{P d_o}{4t}$$

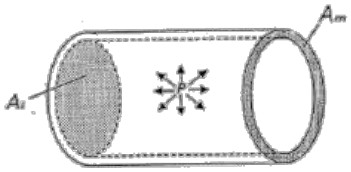

Figure 3. Direction of Force Due to Pipe Pressure

c. Effect of Deflection Moment

$$S_L = \frac{M_b C}{I}$$

Where:

- Ro = outer radius of the pipe
- Z = section modulus (a geometric property of the pipe's cross-section) $= \frac{I}{R_o}$

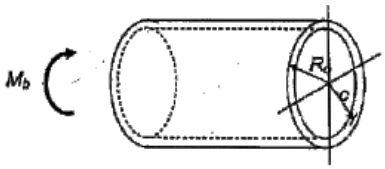

Figure 4. Direction Effect of Pipe Deflection Moment

d. Overall Longitudinal Stress

Overall longitudinal stress can be seen in Figure 5 below:

$$S_L = \frac{F_{ax}}{A_m} + \frac{P d_o}{4t} + \frac{M_b}{Z}$$

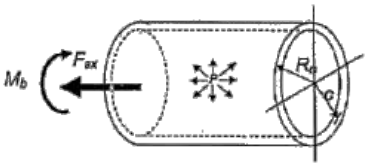

Figure 5. Overall Longitudinal Stress

e. Hoop Stress

$$S_h = \frac{P d_o}{2t}$$

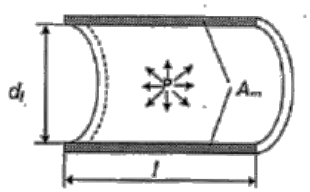

Figure 6. Direction of Circumferential Stress

f. Torsion Moment

$$\tau = \frac{M_T}{2Z_{max}}$$

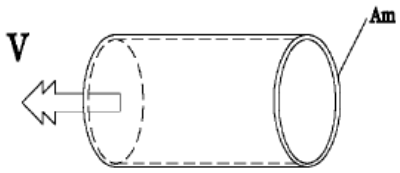

Figure 7. Torsion Moment

2.2 Analysis with ASME B31.1

a. Sustained Load

The stress that occurs due to sustained loads is the total longitudinal stress SL caused by internal pressure, weight, and other sustained loads. This stress must not exceed the allowable stress Sh. It can be expressed mathematically as:

$$SL = \left(\frac{PDo}{4tn}\right) + 1000\left(\frac{0.75iMa}{Z}\right) \leq 1.0Sh$$

b. Occasional Load

The stress that occurs due to occasional loads is the total longitudinal stress caused by internal pressure, weight, and other sustained loads, plus the additional stress from occasional events such as wind or earthquakes. This total stress must not exceed 1.33 times the allowable stress Sh. It can be written mathematically as:

$$So = \left(\frac{PD_o}{4t_n}\right) + 1000\left(\frac{0.75iMa}{Z}\right) + 1000\left(\frac{0.75iMb}{Z}\right) \leq KS_h$$

c. Expansion Load

The stress caused by thermal expansion and/or displacement is referred to as expansion stress Se. This stress arises due to changes in temperature or movement of the piping system, and it is calculated as follows:

$$S_e = 1000\left(\frac{iM_o}{Z}\right) \leq S_a + f(S_h - S_l)$$

This limit ensures that the pipe material can safely withstand the stress caused by thermal growth and displacement cycles without failure due to fatigue or cracking.

$$S_A = f(1.25S_C + 0.25S_h)$$

3. Results and Discussion

3.1 Analysis

To properly design a piping system, every engineer must understand how the system behaves under different loads, as well as the design codes and standards that apply. The behaviours of a piping system can be described using physical parameters such as displacement, acceleration, stress, force, moment, and other related quantities.

Design codes were developed in industrial countries as a response to past failures in piping systems that were not designed safely. Therefore, the main goal of these codes is safety.

Flexibility analysis, as required by the codes, is also aimed at ensuring safety. In general, the main objectives of pipe stress (or flexibility) analysis are:

- To calculate the stress in the pipe and ensure it stays within the allowable limits set by the design codes.
- To calculate the forces acting on equipment nozzles (such as on pressure vessels or tanks) and compare them with the allowable strength of those nozzles.
- To calculate the maximum pipe displacement to prevent interference between pipes or between pipes and nearby structures.
- To optimize the layout and design of pipes and their supports.

3.2 Piping Data Collection

In project design, various supporting documents are needed for the engineering process. These documents are interconnected and serve as simplified summaries of different project specifications and requirements. The key documents include:

- Process Flow Diagram (PFD)
- Piping and Instrumentation Diagram (P&ID)
- Piping Arrangement Drawing
- Isometric Drawing
- Pipe Support Details

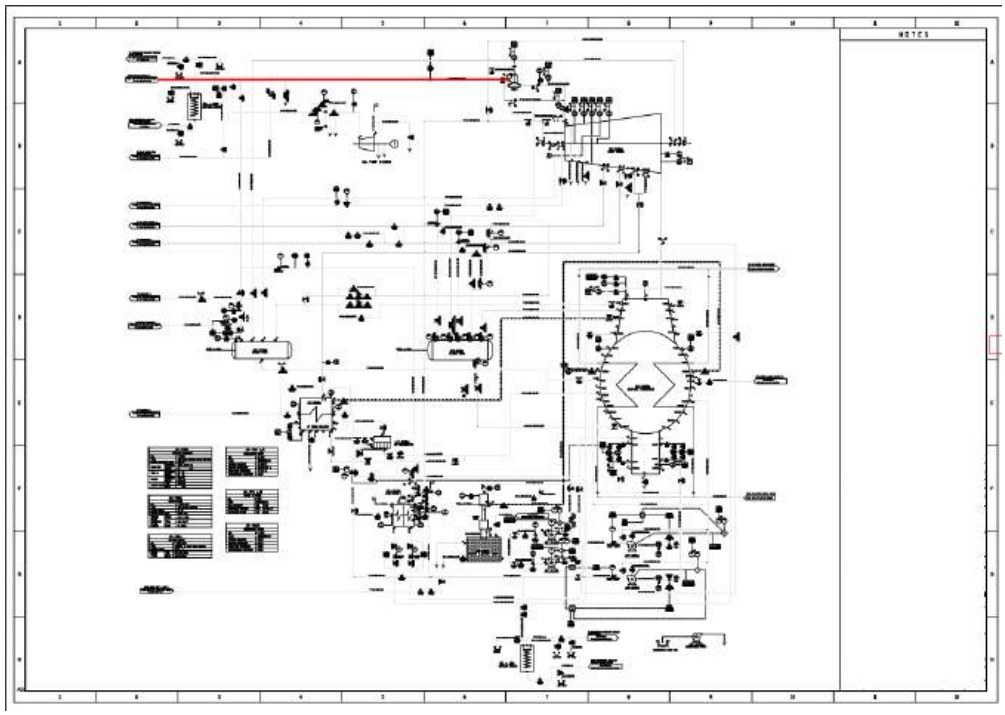

Figure 8. Piping and Instrument Diagram

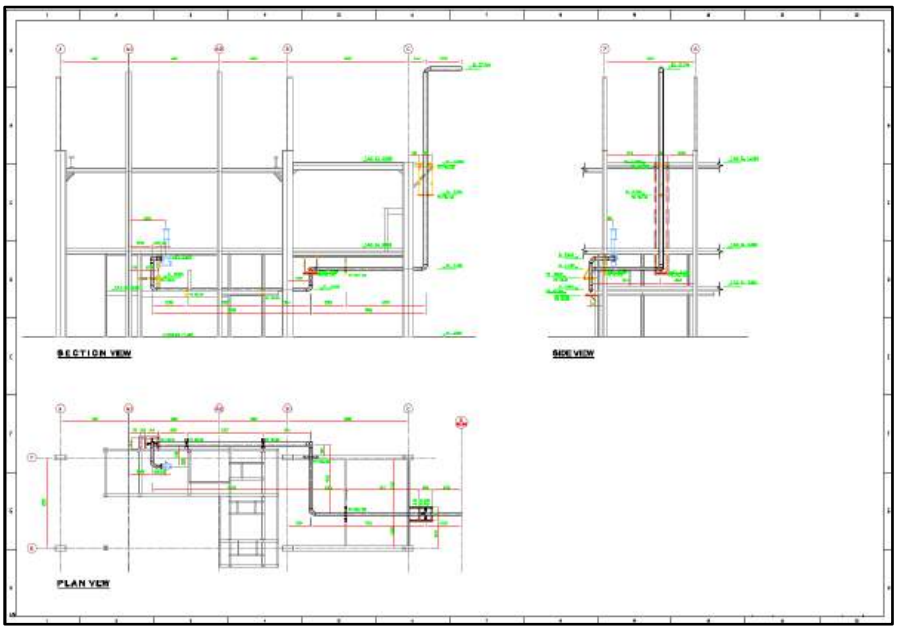

Figure 9. Piping Arrangements Drawing

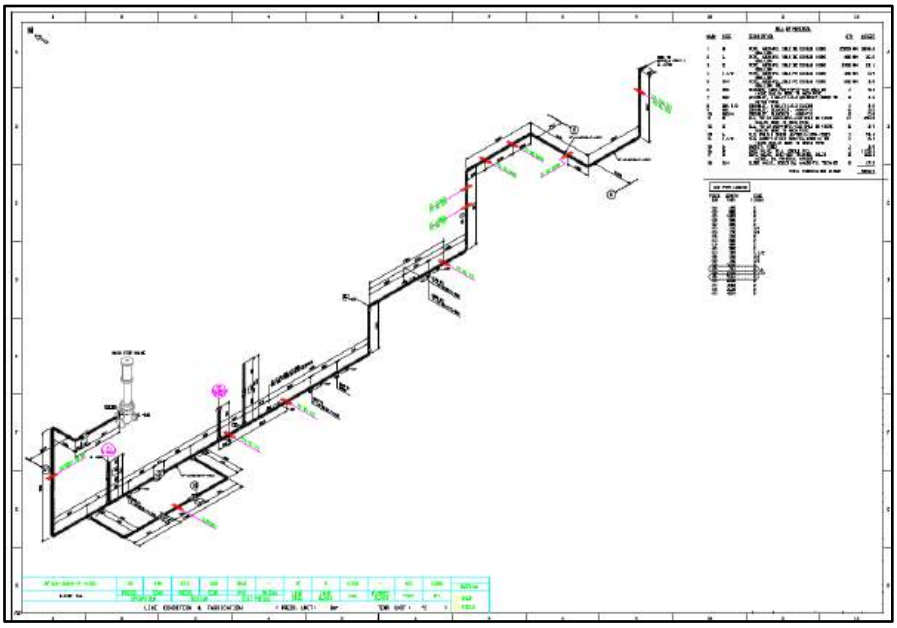

Figure 10. Piping Isometric Drawing

3.3 Piping Data Collection

Table 2. Load Case Definitions

Load Case	Category	Load Combination	Description
1	Hydrotest	L1 = WW + HP	Hydrotest load
2	Operating	L2 = W + T1 + P1 + D1	Load under maximum condition (design pressure & temperature)
3	Operating	L3 = W + T2 + P2 + D2	Load under operating condition with operating pressure & temperature
4	Sustain	L4 = W + P1	Load under maximum condition (design pressure & temperature)
5	Sustain	L5 = W + P2	Load under operating condition with operating pressure & temperature

3.4 Piping Data Collection Pipe Input Data

1) Initial Data Preparation

At this stage, data for the piping system is compiled as the basis for modelling. The necessary data includes piping specifications, and the code standards used.

2) Working Method

The methodology used in completing this paper is an analytical method by modelling the piping system and performing analysis using software CAESAR II. The working method involves literature studies supported by relevant data and expert recommendations.

3) Piping System Modelling

The modelling process includes:

a) Input of node numbers (from node to node)
b) Input of pipe dimensions
c) Input of pipe length and orientation (x, y, z coordinates)
d) Input of pipe material
e) Input of code standard
f) Input of temperature and pressure

4) Error Checking in the Model

a) Physical inspection of the model for drawing errors (coordinate orientation, length dimensions).
b) Running the error check function in CAESAR II to detect modelling errors and warnings.

5) Stress Magnitude Analysis

The magnitude of the loads occurring is analyzed based on the selected code standard (ASME B31.1) using CAESAR II.

6) Explanation of Allowable Stress Types and Load Cases

a) (OPE) Operating: Stress due to a combination of sustained and expansion loads during operational conditions.
b) (OCC) Occasional: Stress occurring during the operational life due to sustained loads combined with occasional loads (such as wind, waves, etc.).
c) (SUS) Sustained: Stress that occurs continuously during operation due to internal pressure and the weight of the pipe and fluid.
d) (EXP) Expansion: Stress resulting from temperature changes.
e) (HYD) Hydrotest: Stress due to water pressure during hydrotesting.

7) Input and Modelling Caesar II

As an engineering, CAESAR II is designed to have standardized input formats. Below are the dominant factors affecting inputs in CAESAR II:

a. Node number input (from node to node)

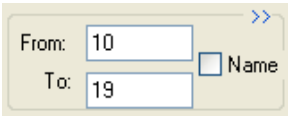

Figure 11. Node Input in CAESAR II

b. Piping design and dimension input

Figure 12. Pipe Dimension Input in CAESAR II

c. Corrosion and insulation input

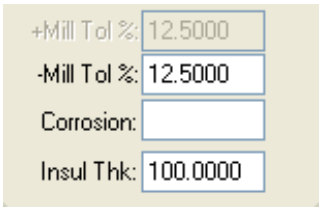

Figure 13. Corrosion and Insulation Input in CAESAR II

d. Temperature and pressure input

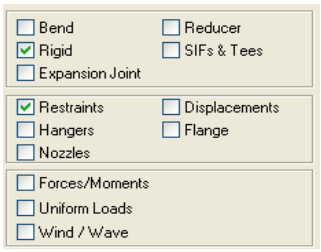

Figure 14. Temperature and Pressure Input in CAESAR II

e. Pipe Support Input

Figure 15. Pipe Support Input in CAESAR II

f. Pipe material input

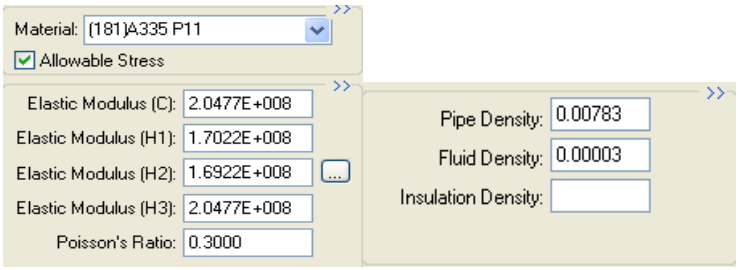

Figure 16. Pipe Material Input in CAESAR II

g. Code standard input

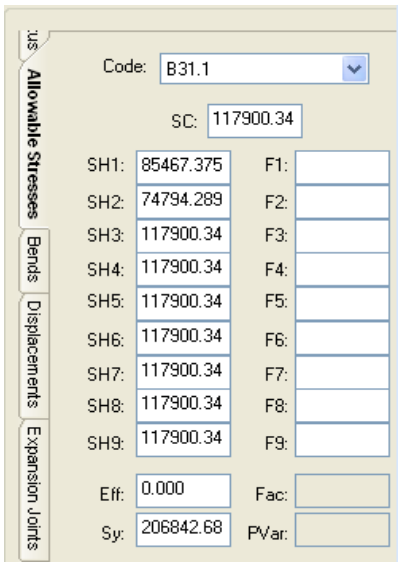

Figure 17. Code Standard Input in CAESAR II

8) Caesar Modelling

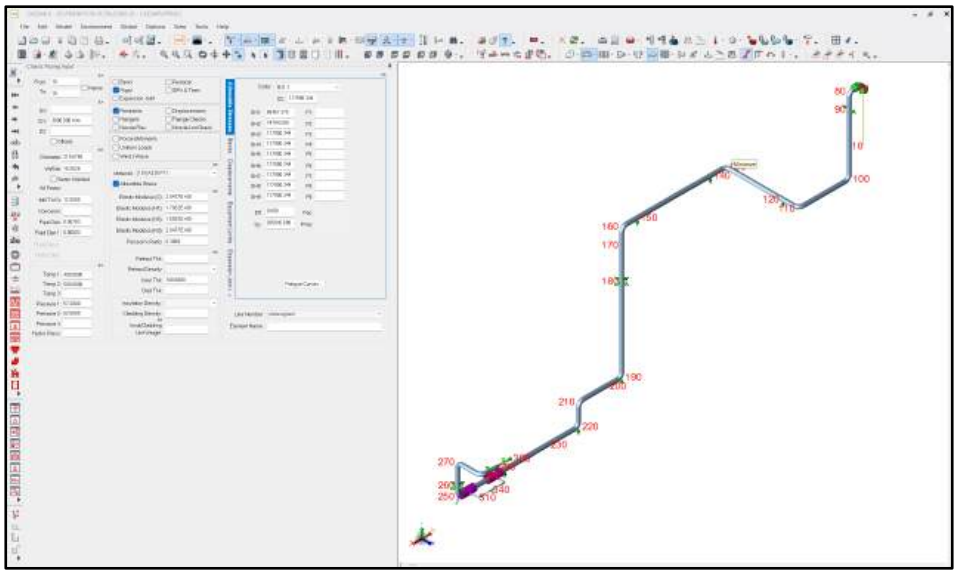

Figure 18. Modelling in CAESAR II

Figure 19 below shows the steam line model, where both ends are connected to a gate valve from the boiler superheater and to the turbine's main steam valve.

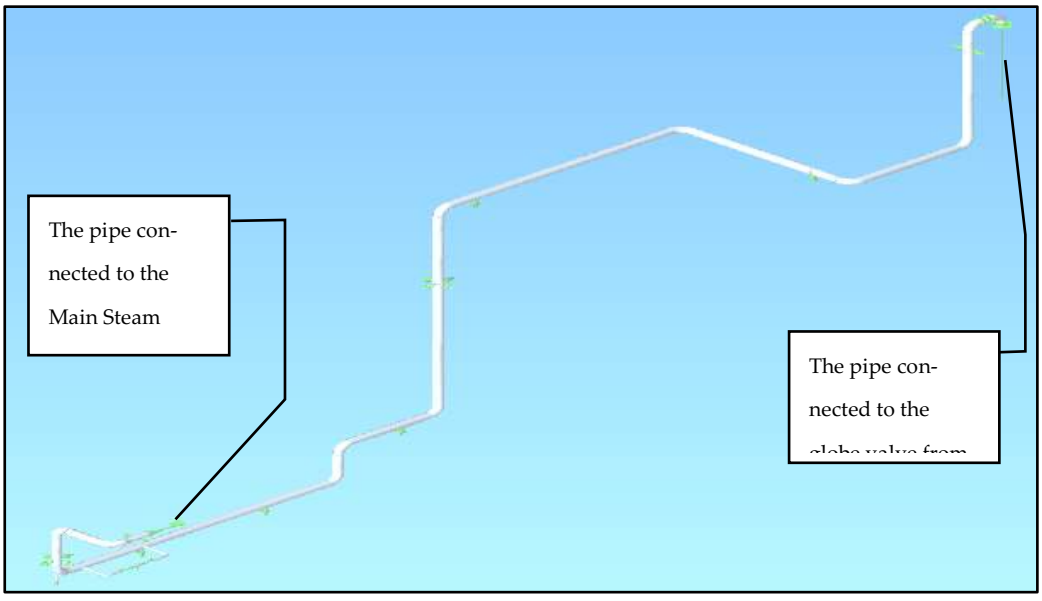

Figure 19. Piping System Caesar Model

3.5 Pipe Stress Results using CAESAR II

The stress analysis results indicate that the piping has sufficient flexibility to avoid overstress. The wall thickness is adequate to withstand the sustained loads, and the pipe supports are sufficient to prevent excessive stress based on ASME B31.1. The Stress Summary results for each load case are shown and summarized in the table below:

Table 3. Code Stress Summary

Case	Category	Load Combination	Node	Max. Stress (Psi)	Allow. Stress (Psi)	%	Status
1	Hydrotest	L1 = WW + HP	249	7260.4	27000	26.9%	Passed
2	Operating	L2 = W + T1 + P1 + D1	159	18908	-	-	Passed
3	Operating	L3 = W + T2 + P2 + D2	159	18472.4	-	-	Passed
4	Sustain	L4 = W + P1	249	7147.1	10848	65.9%	Passed
5	Sustain	L5 = W + P2	249	7146.3	10848	65.9%	Passed
6	Expansion	L6 = L2 - L4	159	18947.4	43484.5	54.4%	Passed
7	Expansion	L7 = L3 - L4	159	18513.6	36779.9	50.3%	Passed

The allowable stress values used as a benchmark in the results above are taken from Appendix Table A-2 of ASME B31.1.

3.6 Pipe Displacement Results using CAESAR II

From the Displacement Report, it can be observed that there are no significant displacements in the pipe system.

Table 4. Maximum Displacement

Case	Max Dx (mm) [Node]	Max Dy (mm) [Node]	Max Dz (mm) [Node]	Remark
Hydrotest	1.35 [270]	-6.2 [290]	-3.89 [290]	Passed
Sustained	-27.49 [130]	68.23 [158]	-68.01 [189]	Passed
Operating	-26.71 [130]	66.25 [158]	-66.37 [189]	Passed

3.7 Pipe Support Load Results using CAESAR II

Table 5. Restraint Summary

NODE	FX lb.	FY lb.	FZ lb.	MX ft.lb.	MY ft.lb.	MZ ft.lb.	Pipe Support Type
10	-2570	-779	-2191	-9099.8	-6349.0	29997.4	Rigid ANC
20	-2570	-779	-2191	12460.7	-6349.0	4703.8	Rigid ANC
90	4074	0	0	0.0	0.0	0.0	Rigid -X
90	0	0	0	0.0	0.0	0.0	Rigid +X
120	-438	-1461	-12	0.0	0.0	0.0	Rigid +Y
140	0	0	0	0.0	0.0	0.0	Rigid +Y
150	0	0	0	0.0	0.0	0.0	Rigid +Y

NODE	FX lb.	FY lb.	FZ lb.	MX ft.lb.	MY ft.lb.	MZ ft.lb.	Pipe Support Type
180	-1315	0	0	0.0	0.0	0.0	Rigid X
180	0	0	-929	0.0	0.0	0.0	Rigid Z
190	0	0	0	0.0	0.0	0.0	Rigid +Y
220	38	-6257	-184	0.0	0.0	0.0	Rigid +Y
240	16	-2337	-68	0.0	0.0	0.0	Rigid +Y
260	0	0	3282	0.0	0.0	0.0	Rigid Z
260	-2354	0	0	0.0	0.0	0.0	Rigid X
288	2286	0	0	0.0	0.0	0.0	Rigid GUI
340	0	0	0	0.0	0.0	0.0	Rigid +Y
2491	296	-1042	101	0.0	0.0	0.0	Rigid +Y

From this table we can see that loading data bigger in node 10 and node 20 mean this node is connection from Boiler. Specifically, this loading data will be use to select and design what kind of pipe support need and can withstand the load.

4. Conclusions

Based on the analysis conducted with CAESAR II on the main steam pipe at Power Plant PLTU Tidore, North Maluku, several important findings were obtained regarding the structural integrity and operational reliability of the piping system.

The piping stress analysis was performed refer to ASME B31.1 for Power Piping design code. The evaluation meets to the and engineering standards. The results indicate that all calculated stress values including sustained stress, thermal expansion stress, and occasional loads are below the allowable limits specified for the pipe (Table-3). This confirms that the piping system is capable of withstanding the applied loads during operation without risk of overstress or material failure.

Others evaluation of the support configuration also shows compliance with the relevant standards. The location, spacing, and type of supports used in the steam pipe is effectively control pipe displacements and loads at critical points (Table-4).

The analysis results demonstrate that the movements occurring along the piping steam system, including thermal expansion and operational displacement, remain within acceptable limits and do not create excessive loads or moments on equipment such as turbines or boilers (Table-5). No significant deformation or misalignment was detected that could lead to leakage, fatigue, or mechanical failure of the piping system.

Therefore, based on these findings, no modification is required regarding the position, distance, or selection of pipe supports. The existing design is considered safe, reliable, and fully compliant with ASME B31.1 standards for the current operating conditions.

References

1. American Society of Mechanical Engineers. (n.d.). *ASME Code B31.1: Power Piping*.
2. Universitas Diponegoro. (2016). Desain dan analisis tegangan sistem perpipaan main steam (high pressure). *Jurnal Teknik Mesin S-1*, 4(1).
3. Nayyar, M. L. (2000). *Piping handbook* (7th ed.). McGraw-Hill.
4. Tambe, P. N., Dhande, K. K., & Jamadar, N. I. (2014). Flexibility and stress analysis of piping system using CAESAR II – Case study. *International Journal of Engineering Research & Technology (IJERT)*, 3(6), 370–373.
5. Intergraph. (2014). *CAESAR II user's guide*. Intergraph.
6. PT. Rekadaya Elektrika. (2013). *PLTU 2×7 MW Tidore, Maluku Utara, Indonesia* [Laporan teknis].
7. Peng, L. C., & Peng, T. L. (2009). *Pipe stress engineering*. American Society of Mechanical Engineers.
8. Kannappan, S. (1986). *Introduction to pipe stress analysis*. John Wiley & Sons.
9. Ferdiansyah, F. (2008). Studi faktor gesek analisa tegangan pada cabang pipa (Skripsi, Fakultas Teknik, Universitas Indonesia).
10. Chamsudi, A. (2005). *Diktat stress analysis*.
11. Raghunandana. (2014). Vibration analysis of a piping system attached with pumps and subjected to resonance. *International Journal of Emerging Technology and Advanced Engineering*, 4.

RiESTech
Recent in Engineering Science and Technology

MBI

Article

Economy Class Passenger Seat Design Concept for Flights in Indonesia

Erwin Nurrizki [1], Agus Edy Pramono [2,*]

[1] Magister Program in Applied Manufacturing Technology Engineering, Politeknik Negeri Jakarta, Jl. Siwabessy, Kampus UI, Depok 16425, Jawa Barat, Indonesia
* Correspondence: agus.edypramono@mesin.pnj.ac.id

Abstract: Aircraft seat bench concept is designed with three adjustment points—armrests, backrest, and the middle of the backrest—and is equipped with a headrest to support the passenger's head and neck comfort. These features aim to enhance passenger comfort without limiting the movement space of neighboring passengers, which is often a concern in conventional aircraft seat designs. To reduce production costs and maintain efficiency, the materials used are commonly available in the market. The seat frame is made of lightweight yet strong aluminum, the seat cushion and backrest utilize polyurethane (PU) foam for comfort, and the outer covering uses synthetic leather, which is affordable yet visually appealing. This material selection facilitates mass production and simplifies maintenance. Structural testing using Autodesk Inventor software indicates that the design is safe for use, achieving a safety factor of 3.62, which signifies strong resistance to stress and load during usage.

Keywords: Aircraft Chair, Economy Class, MSDs, Adjustable chair.

Citation: Nurrizki, E., Pramono, A. E. (2026). Economy Class Passenger Seat Design Concept for Flights in Indonesia. Recent in Engineering Science and Technology, 4(01), 38–43. Retrieved from https://www.mbi-journals.com/index.php/riestech/article/view/114

Academic Editor: Vika Rizkia

Received: 2 Juny 2025
Accepted: 25 November 2025
Published: 31 January 2026

Publisher's Note: MBI stays neutral with regard to jurisdictional claims in published maps and institutional affiliations.

1. Introduction

This design is motivated by the need to improve passenger comfort, especially in economy class which generally has the lowest comfort compared to business class or first class[1]. Economy class passengers often experience discomfort when sleeping during the trip, which not only affects the quality of sleep, but also has the potential to cause disorders of the muscular and skeletal systems (Musculoskeletal Disorders/MSDs). In addition, the position of the head that does not lean properly can disturb other passengers around it. Therefore, redesigning economy class airplane seats by considering ergonomic and comfort aspects is urgently needed.

From this background, the idea emerged to design a more ergonomic and comfortable economy class airplane seat, especially when passengers are in a sleeping position. This design will also allow adjustments to several parts of the seat, such as the headrest and body tilt angle, without disturbing the space of other passengers behind it.

The problems that need to be solved through this design include the need for a new seat design that can improve passenger comfort, the need for an adjustable headrest to reduce the risk of MSDs[2], and a mechanism for adjusting the passenger's body position while sleeping so that it remains comfortable without sacrificing limited cabin space.

The design concept of this chair combines comfort and ergonomics, with the use of materials that are specifically selected to support these functions. The chair frame will be made of strong but lightweight aluminum and composite materials. The seat cushions will use polyurethane foam for comfort, while the outer layer will use synthetic leather that is durable and easy to clean. The structure of the headrest will be made of strong but flexible polycarbonate material to allow for adjustment of the passenger's head position.

Overall, the goal of this design is to create an economy class airplane seat that is not only comfortable to use on long-distance trips, but also able to reduce the possibility of injury or muscle tension due to non-ergonomic sitting or sleeping positions. With the adjuster feature on the backrest and headrest, this chair is expected to provide a more comfortable flying experience for economy class passengers without sacrificing space efficiency in the aircraft cabin.

In previous research, the layout of the aircraft cabin is characterized by the arrangement of components for entertainment or media, for example, the arrangement of monitors, speakers, or control facilities. Arrangement of communication facilities for cabin crew or passengers, Display of navigation data on the monitor for passenger information[3].

Aircraft seat designed with a rail base that allows fore-and-aft movement on the cabin floor rails. Above it is an adjustable seat and backrest, with pivot joints allowing free movement in all directions. The seat is also equipped with adjustable armrests, and an adjustment system for raising or lowering the seat, adjusting the curvature and vertical position of the backrest. All adjustments can be controlled via a panel in the armrest[4].

Next is a passenger seat recline mechanism that includes a fixed seat frame member supporting a pivot axis around which there is a seatback joint and a tray table joint that rotate independently, a seatback pivotally connected to the seatback joint such that the seatback joint rotates forward when the seatback is reclined, and a tray table leg pivotally connected to the tray table joint such that the tray table joint rotates together with the seatback joint when the tray table leg is stowed and rotates independently of the seatback joint when the tray table leg is deployed[5].

2. Materials and Experiment Methods

The design of the economy class airplane seat that has been drafted each has the following specifications:

A. Frame : Aluminum and composite
B. Seat foam : Polyurethane Foam
C. Seat upholstery : Synthetic Leather
D. Headrest structure : Polycarbonate

The reason for choosing these materials is to minimize the budget for making the chair, with common materials available on the market so that it can be considered so that this concept can be continued to the production stage.

The design was analyzed using Autodesk Inventor and Autocad software using the Rapid Upper Limb Assessment (RULA) method to assess ergonomic risks to the upper body. The design was then simulated to measure its performance and comfort. The results of this simulation process form the basis for compiling conclusions and suggestions, which summarize the research results and provide recommendations for further development.

The research begins with observation to understand the initial conditions of the aircraft passenger seat design[6]. After that, problem identification is carried out to find the main issues that need to be addressed in design development. A literature study is then conducted to obtain relevant scientific and technical foundations. Furthermore, data is collected quantitatively and qualitatively to dig deeper into information about passenger needs and comfort. The data obtained is used to analyze passenger sitting postures[7], which are very important in understanding the effect of sitting position on comfort and health, especially on long-haul flights. Based on the results of the analysis, CAD software[8] and the Rapid Upper Limb Assessment (RULA)[9] method will be implemented to assess ergonomic risks to the upper body.

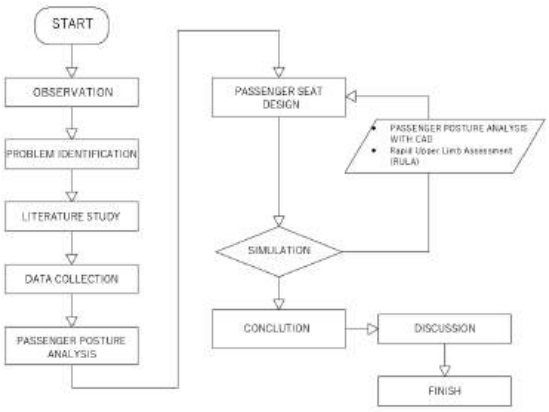

Figure 1. Design Diagram

3. Results and Discussion

3.1. Posture Analysis

Based on the search results regarding the standard airplane seat and comparison with data from one of the Indonesian airlines[10], there is a discrepancy because the author has not found the SNI standard for airplane seats for the Indonesian region, therefore the size of the seat will be adjusted to the reality in the field according to one of the airlines in Indonesia. The following is an ergonomic analysis of the seat. The seat design that is made is simulated with the human position in several conditions.

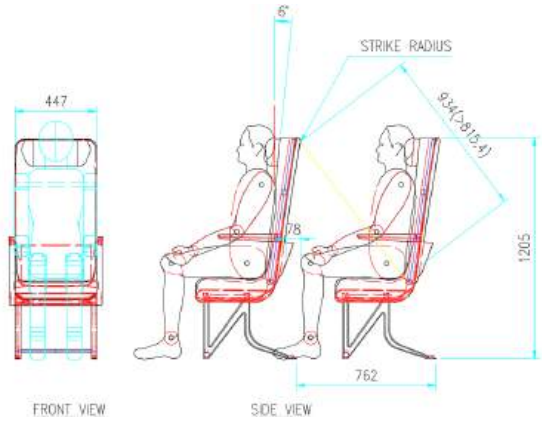

Figure 2. Passenger position when initial conditions, take off, landing, and turbulence

In this position, it can be seen that the passenger is in a comfortable position and the distance between the knee and the front seat is 78 mm, so that the legs still have room to move, then it will be shown when the passenger wants to adjust his sitting position.

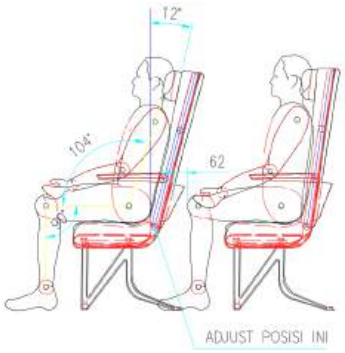

Figure 3. Passenger position when adjusting the seat back

In this position, the passenger angle increases by 6º so that the reclining position can be more comfortable, while the distance between the rear passenger's legs is reduced to 62 mm so that there is still room for the rear passenger to move. Then for the next time when the passenger wants a wider angle, they can adjust the middle part of the backrest

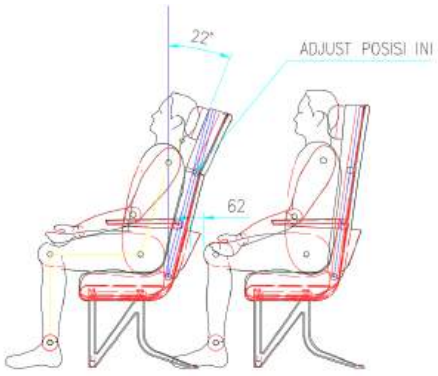

Figure 4. Passenger position when adjusting the middle backrest of the chair

In this position, when the passenger wants to sleep, they can also adjust the headrest to increase comfort, and not disturb the passenger next to them, because sometimes the sleeping passenger will lean against the passenger next to them.

3.2. Load Analysis

The chair was tested for loading assuming a maximum passenger load of 100 kg (1000 N) on the seat base, and a backrest weight of 20 kg (200 N), using Autodesk Inventor software. The following are the test results with the software:

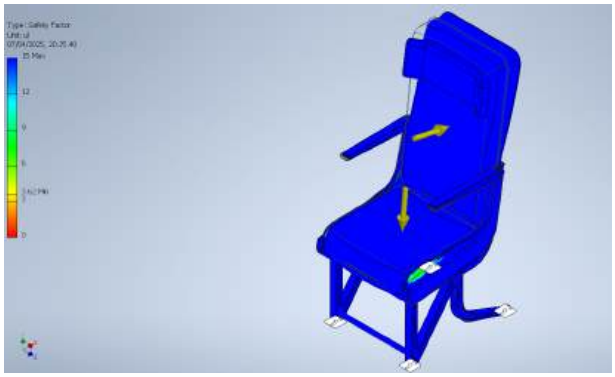

Figure 5. Safety factor test results

A safety factor of 3.62 was obtained, which means it is very safe for passengers because it can be assumed to be able to withstand a load of up to 3.62 times the test load.

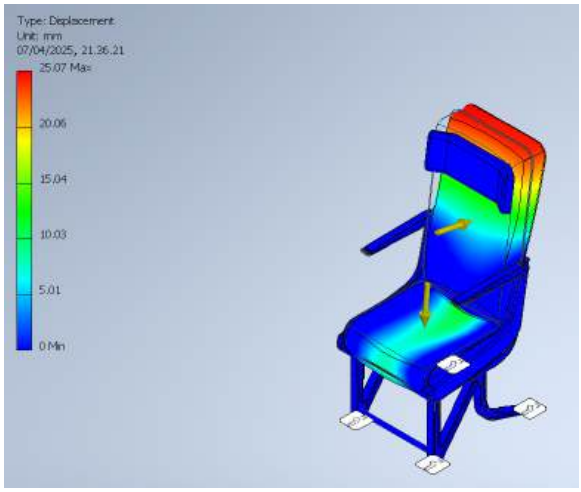

Figure 6. Displacement test results

The displacement that occurred the furthest on the seat back was 25 mm, this is common because the seat must have high deflection to increase passenger comfort.

4. Conclusions

The concept of an airplane seat using 3 adjuster points (armrest, backrest, and middle backrest) and the addition of a headrest can optimize passenger comfort without disturbing other passengers. In this case, to reduce the production budget, the materials used are only common materials on the market such as aluminum frames, PU foam, and synthetic leather can be the solution.

The test results using Autodesk Inventor software show that the design concept is safe to use with a safety factor value of 3.62. In the future, because this is only a concept, R&D is still needed if this will be continued into a product, because it is necessary to test the finished product against the response from correspondence and a feasibility test to be made into a product in accordance with applicable regulations.

References

1. X. Tang *et al.*, "Effect of Airplane Passenger Seat Armrest Height on Human Neck Comfort When Using a Smartphone," *Int. J. Occup. Med. Environ. Health*, vol. 35, no. 2, pp. 199–208, 2022, doi: 10.13075/ijomeh.1896.01874.
2. P. Vink, U. Singh, M. Smulders, G. Vledder, X. Yao, and Y. Song, "Back Rest Angle Influence on Nap Quality and Comfort," *Proc. Hum. Factors Ergon. Soc.*, vol. 67, no. 1, pp. 316–320, 2023, doi: 10.1177/21695067231193754.
3. R. August, "ERGONOMICS GUIDELINES FOR MANUAL HANDLING (second edition)," *Work Safe NB*, no. August, 2011.
4. J. F. Spielman, "AIRCRAFT SEATS AND AIRCRAFT SEATING," 3,019,050, 1962
5. R. J. Suhre and J. W. Hontz, "(12) United States Patent (65) * cited by examiner Prior Publication Data," US 8,870,279 B2, 2014
6. M. Al-Murrakshi, "Seat comfort issues in Economy Class and their effect on long-haul passenger satisfaction and future re-flying intentions," 2021.
7. L. Wang, S. Yu, D. Chen, W. Li, J. Chu, and H. Fan, "Effects of aircraft tray table height and neck posture on passenger comfort: A study of the economy class cabin," *Work*, vol. 75, no. 1, pp. 287–302, 2023, doi: 10.3233/WOR-220043.
8. S. ERDEN and P. YAYLA, "Finite Element Stress Analysis of Airplane Seat," *Eur. Mech. Sci.*, vol. 5, no. 1, pp. 6–13, 2021, doi: 10.26701/ems.799180.
9. A. Gandavadi, J. R. E. Ramsay, and F. J. T. Burke, "EDUCATION VERIFIABLE Assessment of dental student posture in two seating conditions using RULA methodology – a pilot study," 2007, doi: 10.1038/bdj.2007.1047.
10. C. Indonesia, "Armada dan Seating Plan." [Online]. Available: https://www.citilink.co.id/seating-plan/

RiESTech
Recent in Engineering Science and Technology

MBI

Article

Optimization of Bipolar Plate Machining Process Using the Taguchi Method on CNC 3-Axis

Fajar Mulyana [1], Radhi Maladzi [1,*], Bayun Matsaany [1], Nabila Yudisha [1], Muhammad Prasha Risfi [1], Fio Izzafur Rahman [1], Bilal Ramadhan [1], Zezero Meo Cahaya Alam [1]

[1] Applied Bachelor of Manufacturing Technology Engineering, Mechanical Engineering, Jakarta State Polytechnic
* Correspondence: radhi.maldzi@mesin.pnj.ac.id

Abstract: Bipolar plates are critical components in proton exchange membrane fuel cells (PEMFCs), functioning as current collectors and flow field distributors that strongly affect system performance and durability. This study aims to optimize machining time in CNC 3-axis milling of Aluminum Dural 5052 bipolar plates by examining the relationship between machining parameters and material removal rate (MRR). Experimental trials were carried out using a solid carbide end mill with a diameter of 0.7 mm, representing micro-scale machining conditions required for bipolar plate flow field fabrication. Machining time was recorded as the primary response, while MRR was calculated to evaluate machining efficiency. The results show a clear inverse relationship between machining time and MRR. Higher feed rates and greater depths of cut led to increased MRR and reduced machining time. The optimal machining condition was achieved at a spindle speed of 9400 rpm, a feed rate of 100 mm/min, and a depth of cut of 0.4 mm, resulting in the highest MRR of 28.0 mm^3/min and the shortest machining time of 125 minutes. These findings demonstrate that appropriate optimization of machining parameters can significantly enhance machining efficiency while maintaining acceptable process stability, contributing to efficient and cost-effective manufacturing of metallic bipolar plates for PEMFC applications.

Keywords: Bipolar plate; CNC machining; Taguchi method; surface roughness; optimization; PEM fuel cell.

Citation: Mulyana, F., Maladzi, R., Matsaany, B., Yudisha, N., Rifsi, M. P., Rahman, F. I., Ramadhan, B., Alam, Z. M. C. (2026). Optimization of Bipolar Plate Machining Process Using the Taguchi Method on CNC 3-Axis. Recent in Engineering Science and Technology, 4(01), 44–50. Retrieved from https://www.mbi-journals.com/index.php/riestech/article/view/140

Academic Editor: Yudhi Ariadi

Received: 8 Desember 2025
Accepted: 24 January 2025
Published: 31 January 2026

Publisher's Note: MBI stays neutral with regard to jurisdictional claims in published maps and institutional affiliations.

1. Introduction

Proton Exchange Membrane Fuel Cells (PEMFCs) have gained considerable attention as clean and efficient energy conversion systems for automotive, portable, and stationary power applications[1]. Among the key components of a PEMFC stack, bipolar plates play a vital role by serving simultaneously as current collectors, reactant gas distributors, and mechanical supports. The overall performance, efficiency, and durability of PEMFC systems are highly dependent on the design accuracy and manufacturing quality of the bipolar plates, particularly in terms of flow field geometry and surface integrity[2].

In recent years, metallic bipolar plates have been widely investigated as alternatives to conventional graphite plates due to their superior mechanical strength, electrical conductivity, and potential for mass production. Aluminum alloys, especially Aluminum Dural 5052 (AA 5052), have emerged as promising candidates for bipolar plate applications because of their low density, good formability, adequate mechanical properties, and excellent corrosion resistance compared to other aluminum grades[3]. These advantages make AA 5052

particularly attractive for lightweight PEMFC systems, where reduced stack weight and improved manufacturability are critical considerations[4].

CNC machining, particularly 3-axis milling, is commonly employed to fabricate flow field channels on metallic bipolar plates owing to its flexibility and capability to produce complex geometries with high dimensional accuracy. However, the machining of aluminum alloy bipolar plates presents challenges related to productivity, machining time, and process efficiency[5]. Machining time is a crucial factor in bipolar plate manufacturing, as it directly influences production rate, energy consumption, and overall manufacturing cost. Excessive machining time can significantly limit industrial scalability and economic feasibility, especially for high-volume PEMFC production[6].

Machining parameters such as spindle speed, feed rate, and depth of cut play a significant role in determining cutting performance, material removal rate, and total machining time. Inappropriate selection of these parameters may result in inefficient material removal, increased machining time, excessive tool wear, or compromised surface quality. Therefore, optimizing machining parameters to minimize machining time while maintaining acceptable surface finish and dimensional accuracy is essential for enhancing manufacturing efficiency[7].

The objective of this study is to optimize machining time and to investigate its relationship with the material removal rate (MRR) in the CNC 3-axis milling process of Aluminum Dural 5052 bipolar plates. This research systematically analyzes the influence of key machining parameters on machining time and MRR using a structured optimization approach. The optimal machining conditions are identified to minimize process time while maintaining acceptable machining quality. The results of this study are expected to contribute to the development of efficient, lightweight, and cost-effective manufacturing strategies for metallic bipolar plates, thereby supporting the broader adoption of proton exchange membrane fuel cell (PEMFC) technology.

2. Materials and Experiment Methods

Materials

The material used in this study was Aluminum Alloy 5052 (AA 5052), a non-heat-treatable aluminum-magnesium alloy from the 5xxx series, known for its excellent corrosion resistance and moderate mechanical strength. The chemical composition ranges approximately 2.2–2.8% Mg, 0.15–0.35% Cr, and balance Al, with minor amounts of Fe, Si, Cu, Mn, and Zn[8]. Typical mechanical properties for the H32 temper include tensile strength between 228–280 MPa and yield strength ≥193 MPa, with a density of ~2.68 g/cm^3. These attributes make AA 5052 suitable for lightweight metallic bipolar plate manufacturing[9].The cutting tool used in this study is cemented carbide, a hard and wear-resistant material widely utilized in high-precision machining operations. Cemented carbide, also known as tungsten carbide (WC)–cobalt (Co) composite, consists of fine tungsten carbide particles bonded together by a metallic cobalt matrix through a powder metallurgy process.

Experiment Methods

The experimental procedure in this study consists of three main stages: CAD modeling, CAM process planning and G-code generation, and machining parameter optimization using the Taguchi method. Each stage is systematically designed to ensure precision, repeatability, and reliability of the machining process applied to the fabrication of bipolar plates from Aluminum Duralumin 5052.

The first stage involves the creation of a three-dimensional (3D) geometric model of the bipolar plate using SolidWorks, a parametric Computer-Aided Design (CAD) software. The model includes essential design features such as flow channels, inlet and outlet ports, and plate thickness according to the desired specifications for Proton Exchange Membrane (PEM) fuel cell applications. The CAD model serves as the digital representation of the part geometry, which is later used as the input for the Computer-Aided Manufacturing (CAM) stage. The model accuracy directly influences toolpath precision, surface finish, and dimensional conformity of the machined component.

The second stage employs Computer-Aided Manufacturing (CAM) software to convert the 3D CAD model into a machinable toolpath and generate the G-code required for the CNC 3-axis milling machine. The CAM software defines machining parameters such as cutting speed, feed rate, spindle speed, depth of cut, and tool path strategy (e.g., contouring, pocketing, or surfacing). The generated G-code provides the machine control instructions to execute the machining process with high precision and consistency. This stage ensures that the geometric design from the CAD model is accurately replicated in the physical part during CNC machining.

The third stage focuses on the optimization of machining parameters using the Taguchi method, a robust design of experiments (DOE) approach that minimizes variability and enhances process performance with a reduced number of experimental trials. In this study, key machining parameters such as spindle speed (N), feed rate (f), and depth of cut (a) are selected as the control factors, each with predefined levels based on machine and material capabilities. The experiments are arranged according to an orthogonal array (L9, L16, etc.), depending on the number of parameters and levels used[10].

After conducting the machining trials, surface roughness, material removal rate (MRR), and tool wear are measured as the performance responses. The results are analyzed using Signal-to-Noise (S/N) ratios and Analysis of Variance (ANOVA) to identify the most significant parameters and determine the optimal combination of cutting conditions that yield the best machining performance. This integrated experimental methodology—combining CAD design, CAM toolpath generation, and Taguchi-based optimization—provides a systematic framework for improving the machining process of Aluminum Duralumin 5052 bipolar plates. The approach ensures precise fabrication, efficient process control, and scientifically validated optimization of machining parameters under CNC 3-axis milling operations. Experimental methods parameters shown in table 1.

Table 1. shown experimental parameters

Experimental	Spindle Speed (rpm)	Feed Rate (m/min)	Depth of Cut (mm)	Pocket Parameter
1	9400	100	0,4	Paralel Clean Corner
2	9400	90	0,3	Zig-zag
3	9400	80	0,2	Costum Overlap
4	9200	100	0,3	Costum Overlap
5	9200	90	0,2	Paralel Clean Corner
6	9200	80	0,4	Zig-zag
7	9000	100	0,2	Zig-zag
8	9000	90	0,4	Costum Overlap
9	9000	80	0,3	Paralel Clean Corner

After the machining process was completed shown in figure 1, each experimental trial was evaluated based on two primary performance criteria: machining time and surface quality. The machining time represents the process efficiency, reflecting the overall productivity of the operation under the selected cutting parameters. It was measured directly from the CNC machine's operation cycle, encompassing tool engagement, material removal, and tool retraction periods. A shorter machining time indicates higher material removal efficiency and improved process optimization.

Figure 1. Machining Process

Meanwhile, surface quality was assessed in terms of surface roughness (Ra), which serves as a critical indicator of the dimensional accuracy and functional performance of the bipolar plate. Surface roughness measurements were carried out using a contact-type surface roughness tester at multiple locations on each specimen to ensure data reliability and repeatability. Lower surface roughness values correspond to better surface integrity, reduced frictional losses, and enhanced corrosion resistance—attributes that are particularly important for bipolar plates in Proton Exchange Membrane (PEM) fuel cell applications.

Together, these two evaluation parameters—machining time and surface quality—provide a comprehensive understanding of both the efficiency and effectiveness of the machining process. The balance between rapid material removal and superior surface finish

was analyzed to determine the optimal machining parameter combination obtained from the Taguchi experimental design.

3. Results and Discussion

After the machining process, the surface morphology of each specimen was examined using a digital microscope to observe the microstructural characteristics, tool marks, and surface defects generated under different machining parameter conditions. The surface morphology shown in figure 2.

After each machining experiment, the total cycle time was recorded directly from the CNC machine, and the corresponding surface roughness was measured to determine the influence of cutting parameters on machining efficiency and surface quality.

Table 2. Cycle Time and Material Removal Rate

No.	Spindle Speed (rpm)	Feed Rate (mm/min)	Depth of Cut (mm)	Pocket Parameter	Cycle Time (Second)	MRR (mm^3/min
1	9400	100	0,4	Paralel Clean Corner	125	28
2	9400	90	0,3	Zig-zag	155	18,9
3	9400	80	0,2	Costum Overlap	259	11,2
4	9200	100	0,3	Costum Overlap	130	21
5	9200	90	0,2	Paralel Clean Corner	131	12,6
6	9200	80	0,4	Zig-zag	235	22,4
7	9000	100	0,2	Zig-zag	201	14
8	9000	90	0,4	Costum Overlap	230	25,2
9	9000	80	0,3	Paralel Clean Corner	250	16,8

The results obtained from the CNC 3-axis milling experiments demonstrate a clear relationship between machining parameters, material removal rate (MRR), and cycle time in the manufacturing of Aluminum Dural 5052 bipolar plates. As summarized in Table X, variations in feed rate and depth of cut significantly influenced the machining efficiency, which is reflected by changes in MRR and total machining time.

An increase in feed rate generally resulted in a higher MRR, leading to a reduction in cycle time. This trend can be observed by comparing experiments conducted at a feed rate of 100 mm/min with those at 80 mm/min. For instance, Experiment No. 1 achieved the highest MRR of 28.0 mm^3/min with a corresponding cycle time of 125 minutes, whereas Experiment No. 3, conducted at a lower feed rate and shallower depth of cut, resulted in the lowest MRR of 11.2 mm^3/min and the longest cycle time of 259 minutes. This inverse relationship confirms that higher material removal capability contributes directly to improved productivity in milling operations.

Depth of cut also played a crucial role in determining machining performance. Experiments employing a greater depth of cut (0.4 mm) consistently exhibited higher MRR values compared to those using shallower cuts. For example, Experiment No. 8, with a depth of cut of 0.4 mm and a feed rate of 90 mm/min, produced an MRR of 25.2 mm^3/min, which was substantially higher than Experiment No. 5, where a depth of cut of 0.2 mm resulted in an MRR of only 12.6 mm^3/min despite similar machining conditions. These findings indicate that increasing depth of cut is an effective approach to enhance material removal efficiency, provided that surface integrity and tool wear remain within acceptable limits.

Although spindle speed did not directly affect the MRR calculation, its influence on cutting stability and machining time should not be neglected. Slight differences in cycle time were observed among experiments conducted at different spindle speeds, suggesting that spindle speed indirectly affects machining efficiency through its interaction with feed rate and cutting strategy. Additionally, the selected pocket machining strategies (parallel clean corner, zig-zag, and custom overlap) contributed to variations in cycle time, particularly under low MRR conditions, where tool path efficiency becomes more critical.

Overall, the results highlight that machining time is strongly governed by the combined effects of feed rate and depth of cut. Higher MRR values were consistently associated with shorter machining times, emphasizing the importance of parameter optimization for efficient bipolar plate production. From an industrial perspective, minimizing machining time while maintaining acceptable surface finish and dimensional accuracy is essential for improving productivity and reducing manufacturing costs, especially for large-scale PEMFC bipolar plate fabrication.

The findings of this study confirm that systematic optimization of machining parameters in CNC 3-axis milling can significantly enhance process efficiency for Aluminum Dural 5052 bipolar plates. These results provide valuable insights for developing cost-effective and high-throughput manufacturing strategies, supporting the broader adoption of lightweight metallic bipolar plates in PEMFC applications.

4. Conclusions

This study presented an experimental investigation on the optimization of machining time in CNC 3-axis milling of Aluminum Dural 5052 bipolar plates for PEMFC applications. The effects of spindle speed, feed rate, and depth of cut on material removal rate (MRR) and machining time were systematically evaluated using a 0.7 mm diameter solid carbide end mill. The results demonstrated a clear inverse relationship between machining time and MRR, indicating that higher material removal rates effectively reduce cycle time. Feed rate and depth of cut were identified as the most influential parameters governing machining efficiency, while spindle speed exhibited a secondary effect within the investigated range. The optimal machining condition was achieved at a spindle speed of 9400 rpm, a feed rate of 100 mm/min, and a depth of cut of 0.4 mm, yielding the highest MRR of 28.0 mm^3/min and the shortest machining time of 125 minutes.

Although the present study focused on machining time and MRR, further research is required to comprehensively assess machining quality and long-term process reliability.

Future work will investigate the influence of optimized machining parameters on surface roughness, dimensional accuracy, and burr formation in micro-scale flow field channels. In addition, tool wear progression and tool life of small-diameter cutting tools should be examined to ensure process sustainability. Further studies may also incorporate corrosion resistance and surface modification techniques to evaluate the electrochemical performance of machined Aluminum Dural 5052 bipolar plates under PEMFC operating conditions.

References

[1] N. A. A. Qasem, "A recent overview of proton exchange membrane fuel cells: Fundamentals, applications, and advances," Sep. 01, 2024, *Elsevier Ltd*. doi: 10.1016/j.applthermaleng.2024.123746.

[2] Q. Liu, F. Lan, C. Zeng, J. Chen, and J. Wang, "A review of proton exchange membrane fuel cell's bipolar plate design and fabrication process," Aug. 01, 2022, *Elsevier B.V.* doi: 10.1016/j.jpowsour.2022.231543.

[3] T. Zhao, M. A. Islam, X. He, and B. B. Saha, "Application of metallic bipolar plates in PEMFCs: A comprehensive review of performance and durability," Jan. 01, 2026, *Elsevier Ltd*. doi: 10.1016/j.rser.2025.116421.

[4] H. M. Irshad and S. Shahgaldi, "Comprehensive review of bipolar plates for proton exchange membrane fuel cells with a focus on materials, processing methods and characteristics," Mar. 20, 2025, *Elsevier Ltd*. doi: 10.1016/j.ijhydene.2025.02.300.

[5] Z. Xu, D. Qiu, P. Yi, L. Peng, and X. Lai, "Towards mass applications: A review on the challenges and developments in metallic bipolar plates for PEMFC," Dec. 01, 2020, *Elsevier B.V.* doi: 10.1016/j.pnsc.2020.10.015.

[6] S. Porstmann, T. Wannemacher, and W. G. Drossel, "A comprehensive comparison of state-of-the-art manufacturing methods for fuel cell bipolar plates including anticipated future industry trends," Dec. 01, 2020, *Elsevier Ltd*. doi: 10.1016/j.jmapro.2020.10.041.

[7] Y. Xie, S. Mei, and C. Zhang, "Optimisation decision of machining process parameters considering milling energy consumption and specific cutting energy," *Alexandria Engineering Journal*, vol. 128, pp. 786–795, Sep. 2025, doi: 10.1016/j.aej.2025.07.034.

[8] S. A. Farooq *et al.*, "Effect of TiB2 on the mechanical and tribological properties of marine grade Aluminum Alloy 5052: An experimental investigation," *Journal of Materials Research and Technology*, vol. 29, pp. 3749–3758, Mar. 2024, doi: 10.1016/j.jmrt.2024.02.106.

[9] C. Venugopala Chari, B. Pravallika, and M. Bhargava, "Effect of different process parameters on the mechanical properties and microstructural behaviour of AA 5052 welded sheets," *Mater. Today Proc.*, Aug. 2023, doi: 10.1016/j.matpr.2023.08.077.

[10] S. S. Irfan and V. M. Kumar, "'Optimization Of Machining Parameters In Cnc Turning Of En45 By Taguchi's Orthogonal Array Experiments,'" 2019. [Online]. Available: www.sciencedirect.com-www.materialstoday.com/proceedings2214-7853

RiESTech
Recent in Engineering Science and Technology

MBI

Article

Technical and Economic Study of Fast Charging Systems Electric Heavy Equipment in Industrial and Port Areas

Rahmat Noval [1,*], Asep Apriana [1], Fuad Zainuri [1], Dedi Junaedi [1], Fuzi Rachmat Ramdhan [1], Muhammad Hidayat Tullah [2], Danardono Agus Sumarsono [3], Mohammad Adhitya [3]

[1] Program Studi Engineering Technology of heavy equipment maintenance, Department of Mechanical Engineering, Politeknik Negeri Jakarta, Jl. Siwabessy, Kampus, Kampus UI, Depok, 16425, Indonesia
[2] Department of Mechanical Engineering, Politeknik Negeri Jakarta, Jl. Siwabessy, Kampus, Kampus UI, Depok, 16425, Indonesia
[3] Mechanical Engineering Department Faculty of Engineering Universitas Indonesia UI Depok Campus 16424, Indonesia
* Correspondence: rahmat.noval@mesin.pnj.ac.id

Abstract: Despite the increasing adoption of electric heavy equipment in Southeast Asia, there is still limited techno-economic analysis focusing on high-power fast-charging systems tailored for industrial and port operations in emerging economies such as Indonesia. The absence of optimized charging infrastructure results in high downtime, low equipment availability, and uncertain return on investment. The electrification of heavy equipment presents both an opportunity and a challenge for Indonesia's industrial and port operations. Despite advancements in battery energy density and power electronics, the lack of efficient fast-charging infrastructure remains a critical bottleneck. This study evaluates the technical and economic feasibility of implementing high-power DC fast-charging systems for electric heavy machinery in port and industrial settings. Using HOMER Grid and MATLAB-based simulations, three charging configurations (90 kW AC, 250 kW DC, and 500 kW dual-gun DC) were analyzed. Results indicate that the 500 kW system reduces downtime by up to 70%, increasing equipment availability from 75% to 96%. Economic analysis shows a payback period of 4.8 years, internal rate of return (IRR) of 18.7%, and levelized cost of electricity (LCOE) of IDR 2,100/kWh. The findings support the deployment of modular fast-charging hubs to accelerate electrification in logistics and port sectors.

Keywords: Electric heavy equipment; Fast charging; DC-DC converter; Techno-economic analysis; Industrial electrification

Citation: Noval, R., Apriana, A., Zainuri, F., Junaedi, D., Ramdhan, F. R., Tullah, M. H., Sumarson, D. A., Adhitya, M. (2026). Technical and Economic Study of Fast Charging Systems Electric Heavy Equipment in Industrial and Port Areas. Recent in Engineering Science and Technology, 4(01), 51–58. Retrieved from https://www.mbi-journals.com/index.php/riestech/article/view/143

Academic Editor: Noor Hidayati

Received: 4 November 2025
Accepted: 27 November 2025
Published: 31 January 2026

Publisher's Note: MBI stays neutral with regard to jurisdictional claims in published maps and institutional affiliations.

1. Introduction

The global construction and mining sectors are undergoing significant transformation as equipment manufacturers shift toward electric and hybrid drive systems to meet decarbonization targets [1], [2]. In Indonesia, initiatives to adopt electric heavy machinery in industrial and port zones—such as those by SDLG, LiuGong, and SANY—illustrate growing momentum [3].

However, electrification faces two critical challenges: (a) high capital cost and (b) inadequate charging infrastructure [4]. Unlike passenger EVs, heavy-duty machines require large battery capacities (300–600 kWh), making charging time and energy management crucial [5].

This paper presents a techno-economic feasibility study on fast-charging systems for electric heavy equipment in industrial and port operations, focusing on system configuration, operational optimization, and cost-effectiveness.

Previous studies primarily focus on passenger EV charging economics or fleet depot electrification. Limited research evaluates ultra-fast charging systems (≥250 kW) for heavy-duty industrial equipment operating under variable duty cycles in port environments.

However, in Indonesia's port and industrial areas, the electrification of heavy machinery is constrained by three major challenges:

(1) insufficient high-power charging infrastructure,

(2) grid instability under peak charging demand, and

(3) uncertain techno-economic performance under high utilization cycles.

Therefore, this study aims to (1) design and simulate three charging configurations (90 kW AC, 250 kW DC, and 500 kW dual-gun DC), (2) evaluate their technical performance under real port load profiles, and (3) assess their techno-economic feasibility using payback period, IRR, and LCOE indicators.

2. Materials and Experiment Methods

The research employs a mixed-method techno-economic approach that integrates simulation modeling, case studies, and cost analysis.

2.1 System Architecture and Design Framework

Figure 1 illustrates the overall system architecture of the proposed fast-charging system for electric heavy equipment operating in port and industrial environment.

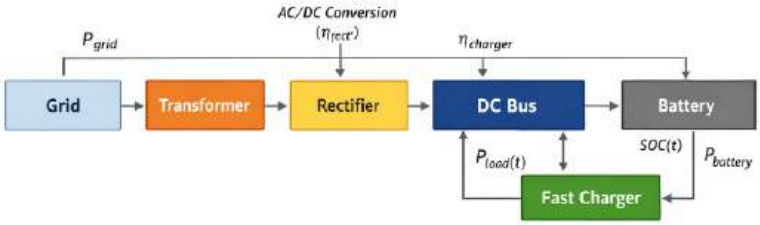

Figure 1. Block diagram of the fast chrging system for elecric heavy equipmen

2.2 Mathematical Modeling and Design Equations

To ensure reproducibility and quantitative evaluation, the proposed fast-charging system was modeled using a physics-based and techno-economic formulation integrating power flow analysis, battery dynamics, and economic performance indicators. The modeling framework captures electrical conversion efficiency, charging energy behavior, load variability, and lifecycle financial metrics

2.2.1 Power Flow Modeling

The instantaneous grid power required to charge the battery is expressed as:

$$P_{grid(t)} = \frac{P_{battery(t)}}{(\eta_{tr} * \eta_{rect} * \eta_{charger})}$$

Where:
P_grid(t) = grid power (kW)
P_battery(t) = battery charging power (kW)
η_tr = transformer efficiency
η_rect = rectifier efficiency
η_charger = charger efficiency

2.2.2 Charging Energy Model

Total charging energy delivered during a charging interval is calculated as:

$$E_{charge} = \int_{t1}^{t2} P_{battery(t)dt}$$

Charging time is determined by:

$$t_{charge} = \frac{\left(C_{bat} * \left(SOC_{final} - SOC_{initial}\right)\right)}{P_{battery}}$$

Where:
C_bat = battery capacity (kWh)
SOC = state of charge (0–1 or %)

2.3 Simulation Environment

The simulation framework was established using MATLAB Simulink and HOMER Grid, enabling a comprehensive techno-economic assessment of electric heavy equipment charging systems under various operational conditions typically found in industrial and port environments. MATLAB Simulink was utilized to model the dynamic power flow, charging behavior, and battery thermal characteristics, whereas HOMER Grid was employed to evaluate system-level energy optimization, grid interaction, and economic feasibility based on tariff structures and load profiles.

Three distinct charging configurations were analyzed to capture the performance differences across various power delivery architectures:

1. AC Slow Charger (90 kW) – representing a conventional grid-connected charging system commonly adopted for depot-based charging or overnight operations. This configuration serves as a baseline scenario, emphasizing lower infrastructure cost but longer charging duration and higher idle time for equipment.
2. DC Fast Charger (250 kW) – simulating a high-power charging architecture capable of reducing downtime and improving fleet utilization in high-duty cycle applications. The DC fast charger model included detailed rectifier efficiency, power factor correction, and cable loss components to reflect realistic field performance.
3. Dual-Gun DC Fast Charger (500 kW) – representing an advanced configuration where simultaneous charging of two heavy-duty vehicles is enabled, or alternatively, ultra-fast single-vehicle charging for high-capacity battery systems (>600 kWh). This configuration was modeled to assess the limits of grid integration, transformer loading, and harmonic distortion under transient demand conditions.

Each configuration was evaluated within a 24-hour operational cycle typical of port and industrial logistics activities, where load patterns exhibit high variability due to equipment utilization during loading/unloading and shift transitions. The simulation time step was set to one minute to capture transient events in current and voltage fluctuations, while the ambient temperature profile was also incorporated to simulate battery performance degradation and charging efficiency variations.

In HOMER Grid, the corresponding power flow data from MATLAB Simulink were integrated to perform energy dispatch optimization involving grid electricity, renewable inputs (where applicable), and potential energy storage systems. The optimization aimed to minimize the Levelized Cost of Charging (LCOC) while ensuring grid stability and compliance with local utility constraints.

This hybrid modeling approach allowed for an in-depth comparison not only of technical parameters—such as efficiency, peak demand, and thermal loading—but also of economic metrics, including payback period, net present cost (NPC), and operational expenditure (OPEX). Consequently, the simulation environment provided a robust foundation for subsequent analysis in Section 3, focusing on performance benchmarking and financial viability of fast-charging systems for electric heavy equipment in industrial and port areas.

2.4 Operational Load Profile Modeling

Industrial and port operations exhibit fluctuating charging demand due to multi-shift logistics activity. The aggregated charging demand for multiple units operating in port environments is defined as

$$P_{load(t)} = \Sigma_{i=1}^{n}\left(P_i * U_{i(t)}\right)$$

Where:
P_i = rated charging power of unit i
U_i(t) = utilization factor (0–1)
n = number of active charging unit

1. Locations: Tanjung Priok Port and Karawang Industrial Estate.
2. Equipment: Electric wheel loaders, reach stackers, and container handlers.

2.5 Economic Modeling and Performance Indicator

2.5.1 Economic Performance Modeling

Levelized Cost of Charging (LCOC) is calculated as:

$$LCOC = \frac{(CAPEX * CRF + OPEX)}{E_{annual}}$$

Where:
CAPEX = capital expenditure
OPEX = annual operational cost
E_annual = annual energy delivered

2.5.2 Performance Indicator

1. Tariff: IDR 1,600/kWh (industrial rate)
2. Utilization: 3,000 hours/year
3. Charger efficiency: 92%
4. Discount rate: 8%
5. System lifetime: 10 years.

2.6 Environmental Impact Assessment

CO_2 reduction potential was calculated using emission factors from the International Energy Agency (IEA) [6]. considering regional grid emission intensities and the energy mix composition dominated by coal, natural gas, and renewables. The assessment aimed to quantify the environmental benefits of electrifying heavy equipment operations in industrial and port zones, where diesel combustion engines are traditionally major contributors to local air pollution and greenhouse gas (GHG) emissions.

Furthermore, lifecycle emission analysis was also incorporated by considering charger manufacturing, installation, and maintenance footprints, derived from Ecoinvent database factors. Although initial embodied emissions for fast-charging infrastructure were higher than those of slow-charging systems, the overall carbon payback period was observed to be less than 1.8 years for the 500 kW configuration—highlighting the substantial long-term sustainability advantages.

The resulting CO_2 reduction profiles not only reinforce the technical viability of fast-charging systems for electric heavy equipment but also demonstrate strong alignment with global decarbonization pathways, such as the IEA Net Zero 2050 scenario and the IMO (International Maritime Organization) port decarbonization framework. These findings underline the strategic potential of implementing high-power charging networks as a critical enabler of sustainable industrial electrification.

3. Result and Discussion

3.1 Technical Feasibily

Tabel 1. Simulation results show that charging performance improves dramatically with higher power configurations

System	Power (kW)	Charging Time (20%-100%)	Availability	Efficient (%)
AC 90 kW	90	6.0 h	75%	88
DC 250 kW	250	2.4 h	905	90
DC 500 kW	500	1.4 h	96%	92

High-power systems maintain thermal stability within limits (battery <45°C), supporting frequent operations in port cycles. The dual-gun architecture also allows simultaneous dual equipment charging, enhancing throughput by 25% [7]

3.2 Economic Analysis

Capital cost for a 500 kW system is estimated at IDR 3.2 billion, including power electronics, cooling, and grid connection.Operational costs are dominated by energy consumption and maintenance (IDR 150 million/year).

As shown in Table 2, payback occurs within 4.8 years with IRR of 18.7%.

Parameter	Unit	Value
CAPEX	IDR	3.2 Billiom
OPEX	IDR/Year	150 Million
Payback Period	Years	4.8
IRR	%	18.7
LCOE	IDR/kWh	2.100

These results align with international findings on **fast-charging economics** for heavy-duty EVs [8], [9]. The adoption **of solar-assisted charging microgrids** could further reduce LCOE to IDR 1,700/kWh [10].

3.3 Environmental Impact

Each 400 kWh electric wheel loader reduces annual CO_2 emissions by approximately 29 tons, displacing 11,000 liters of diesel fuel [11].

If deployed at scale in ports such as Tanjung Priok and Belawan, total emission reduction could reach 12,000 tons CO_2/year [12].

3.4 Challenges

Key implementation barriers include:

1. Limited **grid capacity and transformer availability** [13].
2. Lack of **national fast-charging standards for industrial equipment** [14].
3. Need for **workforce training in high-voltage maintenance** [15].

The transition toward electric heavy equipment in industrial and port areas faces multifaceted technical and institutional barriers that must be systematically addressed to ensure reliable deployment. The limited grid capacity remains the most critical constraint, as existing distribution networks in industrial zones were primarily designed for steady-state power demands rather than highly dynamic, high-peak charging loads. The introduction of multiple DC fast chargers—particularly in the 250 to 500 kW class—can cause transformer overloading, voltage sag, and harmonic distortion, leading to power quality issues that affect both the charging system and surrounding industrial operations. To mitigate this, smart load management systems, demand response algorithms, and the integration of on-site energy storage systems (ESS) have been proposed. These strategies help flatten load profiles and reduce peak power draw from the grid, enabling smoother

integration without costly substation upgrades.

Finally, environmental and spatial constraints also need consideration, particularly in port areas where salt corrosion, dust ingress, and limited installation space demand ruggedized, compact charger designs with IP65-rated enclosures and liquid-cooled cabling systems. Future infrastructure planning must integrate environmental resilience as a design criterion to ensure long-term operational reliability under heavy-duty cycles.

In summary, overcoming these implementation barriers requires a multidimensional strategy encompassing grid modernization, regulatory standardization, and capacity building. By aligning technical solutions with institutional frameworks, industrial and port operators can accelerate the adoption of fast-charging systems for electric heavy equipment, paving the way toward sustainable, low-emission industrial ecosystems.

3.5 Comparative Benchmarking

Compared to the 90 kW system, the 500 kW configuration reduces charging time by 76%, increases equipment availability by 21%, and improves IRR by 6.3%

4. Conclusions

This study confirms that 500 kW dual-gun DC fast-charging systems are both technically feasible and economically viable for port and industrial applications in Indonesia. They enable a 70% reduction in downtime, 96% equipment availability, and payback within 5 years.

This study successfully achieved its objectives by:

1. Development of shared charging hubs across industrial clusters.
2. Integration with renewable energy microgrids.
3. Government-backed incentives and regulatory frameworks for infrastructure deployment.

Funding
This study received no specific funding from government, commercial, or non-profit organizations.

Acknowledgments
The authors would like to thank **Politeknik Negeri Jakarta** and **Universitas Indonesia** for research collaboration and technical laboratory support.

References

[1] A. Kumar et al., "Electrification of construction equipment: Challenges and opportunities," *Energy Reports*, vol. 8, pp. 3541–3553, 2022.

[2] Volvo CE, "The future of construction equipment electrification," *Technical White Paper*, 2023.

[3] Equipment Indonesia, "Electric and Hybrid Heavy Equipment Trends," *EIM Magazine*, Oct. 2025.

[4] R. P. Sari, "Economic barriers in the electrification of heavy machinery," *J. Eng. Energy Technol.*, vol. 17, no. 3, 2024.

[5] M. J. Ehsani et al., *Modern Electric, Hybrid, and Fuel Cell Vehicles*, CRC Press, 2021.

[6] International Energy Agency (IEA), "Global EV Outlook 2024," IEA Report, 2024.

[7] H. Wang et al., "Fast charging strategies for lithium-ion batteries in industrial applications," *IEEE Trans. Ind. Electron.*, vol. 70, no. 9, pp. 9740–9752, 2023.

[8] A. K. Jaiswal, "Economic viability of fast chargers for heavy EVs," *Renewable Energy*, vol. 210, pp. 480–491, 2024.

[9] Y. Zhao et al., "High-power DC charging architectures," *IEEE Trans. Power Electron.*, vol. 38, no. 5, pp. 5101–5112, 2023.

[10] L. Zhang et al., "Hybrid solar-grid fast charging stations," *Applied Energy*, vol. 330, 2023.

[11] S. Gupta et al., "Decarbonizing construction with electric heavy equipment," *J. Clean. Prod.*, vol. 420, 2024.

[12] Ministry of Transportation, "Sustainable Port Operations Report," Jakarta, 2024.

[13] PLN Indonesia, "Industrial Grid Capacity Analysis," Technical Report, 2024.

[14] B. Subekti, "Standardisasi sistem pengisian cepat alat berat listrik," *Teknika J. Energi Terbarukan*, vol. 6, no. 2, 2025.

[15] P. Li and X. Chen, "Safety protocols for high-voltage heavy-duty charging," *IEEE Access*, vol. 12, pp. 17720–17732, 2024.

[16] LiuGong, "Smart factory and MES integration," *LiuGong Whitepaper*, 2024.

[17] SANY Group, "Hybrid powertrain innovation roadmap," *SANY Technical Bulletin*, 2023.

[18] SDLG Indonesia, "L980HEV technical overview," Product Brief, 2025.

[19] A. Nugroho et al., "Microgrid applications for industrial electrification," *Indonesian J. Energy Eng.*, vol. 11, no. 1, 2024.

[20] Konecranes, "TRUCONNECT telematics system for port cranes," Tech. Doc., 2025.

PT. Mencerdaskan Bangsa Indonesia

PT MENCERDASKAN BANGSA INDONESIA
(MBI), 4th Floor Gedung STC Senayan Room
31-34, Jl. Asia Afrika Pintu IX, Jakarta 10270,
Indonesia.